AD-A191 602 ELECTROMAGNETIC PENETRATION INTO A CONDUCTING CIRCULAR CYLINDER THROUGH A.. (U) SYRACUSE UNIV NY DEPT OF ELECTRICAL AND COMPUTER ENGINEERING.. J R MAUTZ ET AL. 1/1

UNCLASSIFIED NOV 87 SYRU/DECE/TR-87/4 ARO-21370.11-EL F/G 20/3 NL

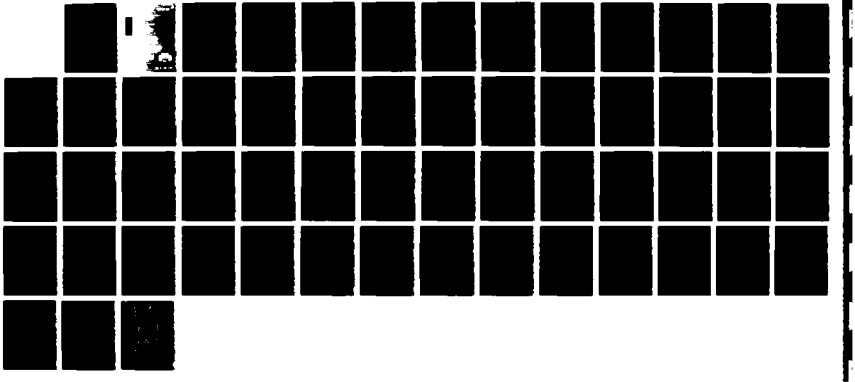

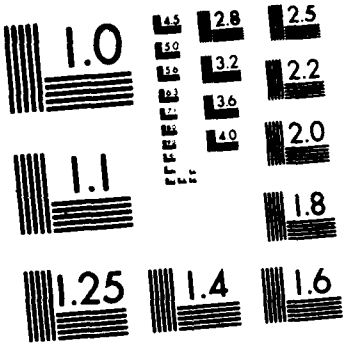

SYRU/DECE/TR-87/4

# ELECTROMAGNETIC PENETRATION INTO A CONDUCTING CIRCULAR CYLINDER THROUGH A NARROW SLOT, TE CASE

Interim Technical Report No. 8

by

Joseph R. Mautz
Roger F. Harrington

November 1987

Department of
Electrical and Computer Engineering
Syracuse University
Syracuse, New York 13244-1240

Contract No. DAAG29-84-K-0078

Approved for public release; distribution unlimited



Prepared for

ARMY RESEARCH OFFICE
RESEARCH TRIANGLE PARK
NORTH CAROLINA 27709

UNCLASSIFIED

SECURITY CLASSIFICATION OF THIS PAGE (When Data Entered)

| REPORT DOCUMENTATION PAGE | | READ INSTRUCTIONS BEFORE COMPLETING FORM |
|---|---|---|
| 1. REPORT NUMBER ARO 21378.11-EL | 2. GOVT ACCESSION NO. | 3. RECIPIENT'S CATALOG NUMBER |
| 4. TITLE (and Subtitle) ELECTROMAGNETIC PENETRATION INTO A CONDUCTING CIRCULAR CYLINDER THROUGH A NARROW SLOT, TE CASE | | 5. TYPE OF REPORT & PERIOD COVERED Interim Technical Report #8 |
| | | 6. PERFORMING ORG. REPORT NUMBER |
| 7. AUTHOR(s) Joseph R. Mautz<br>Roger F. Harrington | | 8. CONTRACT OR GRANT NUMBER(s) DAAG29-84-K-0078 |
| 9. PERFORMING ORGANIZATION NAME AND ADDRESS<br>Department of Electrical & Computer Engineering<br>Syracuse University<br>Syracuse, New York 13244-1240 | | 10. PROGRAM ELEMENT, PROJECT, TASK AREA & WORK UNIT NUMBERS |
| 11. CONTROLLING OFFICE NAME AND ADDRESS<br>U.S. Army Research Office<br>Post Office Box 12211<br>Research Triangle Park, NC 27709 | | 12. REPORT DATE November 1987<br>13. NUMBER OF PAGES 54 |
| 14. MONITORING AGENCY NAME & ADDRESS(if different from Controlling Office) | | 15. SECURITY CLASS. (of this report) UNCLASSIFIED<br>15a. DECLASSIFICATION/DOWNGRADING SCHEDULE |

16. DISTRIBUTION STATEMENT (of this Report)

Approved for public release; distribution unlimited

17. DISTRIBUTION STATEMENT (of the abstract entered in Block 20, if different from Report)

NA

18. SUPPLEMENTARY NOTES

The view, opinions, and/or findings contained in this report are those of the author(s) and should not be construed as an official Department of the Army position, policy, or decision, unless so designated by other documentation.

19. KEY WORDS (Continue on reverse side if necessary and identify by block number)

Aperture problems
Circular cylinder
Electromagnetic penetration
Magnetic current
Numerical solution
Resonance
TE Case

20. ABSTRACT (Continue on reverse side if necessary and identify by block number)

A procedure is presented for calculating the electromagnetic field in the vicinity of an infinitesimally thin conducting circular cylindrical shell with an infinitely long slot illuminated by a TE plane wave. This field is the short-circuit field plus the field due to the slot. The short-circuit field is the field that would exist if there were no slot. The field due to the slot stems from the $\phi$ component of the electric field in the slot. Approximated by a linear combination of expansion functions that satisfy the

DD FORM 1 JAN 73 1473 EDITION OF 1 NOV 65 IS OBSOLETE
S/N 0102-014-6601

UNCLASSIFIED
SECURITY CLASSIFICATION OF THIS PAGE (When Data Entered)

20. ABSTRACT (continued)

edge conditions, this field component is determined by testing the equation of continuity of the axial magnetic field in the slot with non-negative powers of $\phi$ where $|\phi|$ is the angular distance from the center of the slot.

Alternative expansion functions are introduced to preserve the accuracy of the solution in the vicinity of an internal resonance. Containing the resonant electric field, the first alternative expansion function is normalized so that its axial magnetic field remains finite as the resonant frequency is approached. The resonant electric field is that interior electric field whose $\phi$ component approaches zero on the closed surface consisting of the cylindrical shell and the slot as the frequency approaches the resonant frequency. The rest of the alternative expansion functions are orthogonal to the resonant electric field.

CONTENTS

## I. INTRODUCTION

Scattering of a TE electromagnetic wave by a conducting circular cylinder with an infinitely long axial slot was computed in [1] and [2] by three different methods: numerical solution of the aperture field integral equation, numerical solution of the electric field integral equation, and numerical solution of the magnetic field integral equation. The method of numerical solution of the electric field integral equation was also used in [3]. When the slot is so narrow that the field inside the cylinder is a small fraction of the incident field, the field inside the cylinder can not be accurately determined by the method of numerical solution of the electric field integral equation because, in this method, the field inside the cylinder is the sum of the incident field and the field due to the numerically calculated electric current on the surface of the cylinder. The incident field is the field that would exist if the cylinder were absent. Similarly, numerical solution of the magnetic field integral equation will not accurately determine the field inside the cylinder when this field is a small fraction of the incident field. Furthermore, the magnetic field integral equation applies only to a conducting cylindrical shell of finite thickness. The scattering problem was also formulated as a dual series problem and solved by techniques borrowed from the Riemann-Hilbert problem in complex variable theory [4]-[8].

In the present report, we solve the problem of scattering by an infinitesimally thin conducting circular cylindrical shell with a narrow but infinitely long slot by means of the aperture field integral equation. As in [2], we use the method of moments to obtain a numerical solution of the aperture field integral equation. In contrast to the pulse expansion functions and point testing functions used in [1], we use expansion

functions that satisfy the edge conditions and test with non-negative powers of $\phi$ where $|\phi|$ is the angular distance from the center of the slot aperture. In comparison with [9, pp. 1392-1398] where only one expansion function is used, the aperture field integral equation is point matched, and no numerical calculations are performed, we use up to 4 expansion and testing functions and calculate fields at the center of the cylinder and at the center of the slot aperture.

In our formulation, the elements of the moment matrix are evaluated by replacing each expansion function by a very large but finite number of terms in its Fourier series with respect to $\phi$. Bessel functions of large order are approximated by means of Debye's asymptotic expansions [10,p. 366]. To obtain a moment matrix that remains well-conditioned as the frequency approaches a resonant frequency of the associated cavity, we choose expansion functions so that the magnetic field of only one of them contains the resonant magnetic field. The associated cavity is the cavity enclosed by the complete circular cylindrical surface. The complete circular cylindrical surface is the conducting shell with the slot covered by a conducting surface whose radius of curvature is the same as that of the shell. The magnetic field of an aperture electric field expansion function is the magnetic field that exists inside the cylinder when the tangential electric field vanishes on the conducting circular cylindrical shell and is equal to the expansion function in the slot. The resonant magnetic field is the magnetic field associated with the resonant electric field. The resonant electric field is the interior electric field whose $\phi$ component approaches zero on the complete cylindrical surface as the resonant frequency is approached.

So constructed, our moment solution remains accurate when the associated cavity is resonant. A computer program was written to implement our solution. This computer program will be described and listed in a forthcoming report.

## II. MATHEMATICAL FORMULATION

The formulation for the TE excited cylindrical shell is similar to that for the TM excited cylindrical shell in [11]. Furthermore, the computer program that was written to implement it is similar to the one in [12]. An infinitesimally thin, perfectly conducting circular cylindrical shell of radius a having a slit aperture of half angle $\phi_o$ is illuminated by a TE polarized plane wave. In terms of the polar coordinates $(\rho,\phi,z)$, the equation of the shell is $(\rho=a,\ \phi_o \leq \phi \leq 2\pi-\phi_o)$ and the incident magnetic field $\underline{H}^i$ is taken to be

$$\underline{H}^i = \underline{u}_z e^{jk\rho\cos(\phi-\alpha)} \tag{1}$$

where a time factor $e^{j\omega t}$ has been assumed and suppressed. See Fig. 1. The incident magnetic field is the magnetic field that would exist if the shell were absent. In (1), $\underline{u}_z$ is the unit vector in the z direction, $\alpha$ is the angle of the direction from which the incident wave comes, and $k = \omega\sqrt{\mu\varepsilon}$ is the wave number where $\mu$ and $\varepsilon$ are, respectively, the permeability and permittivity of the medium surrounding the shell. Our objective is to find the electric and magnetic fields everywhere in Fig. 1.

We close the aperture with an infinitely thin curved conducting strip whose equation is $(\rho=a,\ |\phi| \leq \phi_o)$ and, as shown in Fig. 2, we place the magnetic current $\underline{M}$ on the right-hand side of the closed aperture and $-\underline{M}$ on the left-hand side of the closed aperture. These magnetic currents

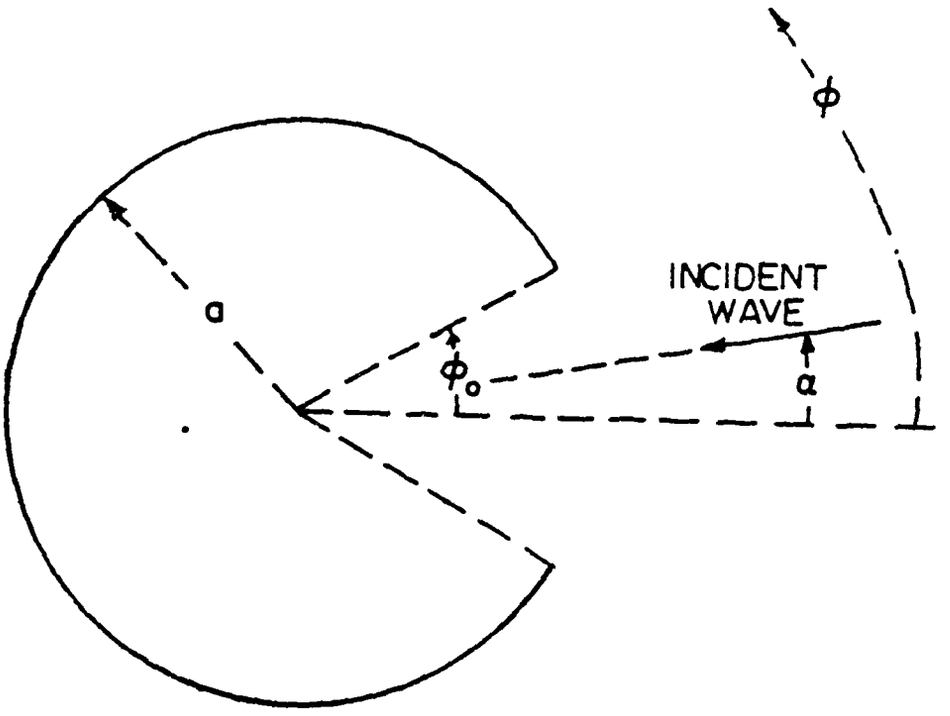


Fig. 1. The geometry.

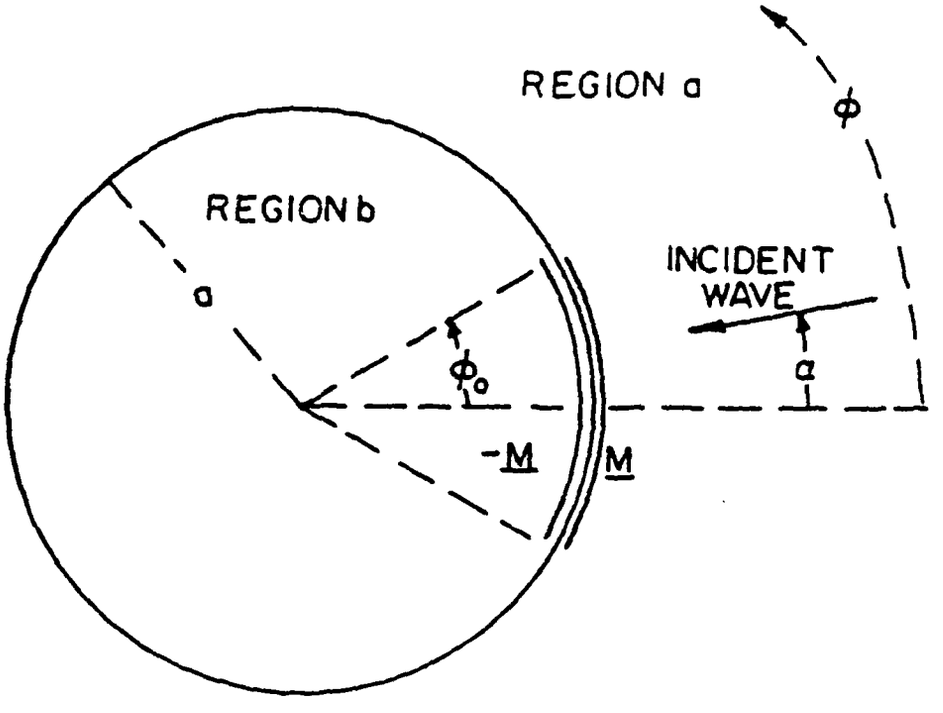


Fig. 2. Equivalent Situation.

restore the tangential electric field in the aperture. The situation in Fig. 2 will be equivalent to that in Fig. 1 if the tangential magnetic field is continuous across the closed aperture. Thus, since the magnetic field of a TE wave is in the z direction, we require that

$$H_z^b(-\underline{M}) = H_z^a(\underline{M}) + H_z^{sc} \quad , \quad \begin{cases} \rho = a \\ |\phi| \leq \phi_o \end{cases} \tag{2}$$

where $\underline{u}_z H_z^b(-\underline{M})$ is the magnetic field due to $-\underline{M}$ placed on the region b side of the closed aperture in Fig. 2, $\underline{u}_z H_z^a(\underline{M})$ is the magnetic field due to $\underline{M}$ placed on the region a side of the closed aperture in Fig. 2, and $\underline{u}_z H_z^{sc}$ is the magnetic field that would exist if the incident wave impinged on the conducting shell with its aperture closed, i.e., on the conducting circular cylinder of radius a. Region a is the region for which $\rho \geq a$. Region b is the region for which $\rho \leq a$.

Equation (2) is recast as

$$H_z^b(-\underline{M}) - H_z^a(\underline{M}) = H_z^{sc} \quad , \quad \begin{cases} \rho = a \\ |\phi| \leq \phi_o \end{cases} \tag{3}$$

We let

$$\underline{M} = \underline{u}_z(M^e + M^o) \tag{4}$$

where $M^e$ is even in $\phi$ and $M^o$ is odd in $\phi$. Because the magnetic field due to $\underline{u}_z M^e$ is even in $\phi$ and that due to $\underline{u}_z M^o$ is odd in $\phi$, (3) decomposes into

$$H_z^b(-\underline{u}_z M^e) - H_z^a(\underline{u}_z M^e) = H_z^{sce}, \quad \begin{cases} \rho = a \\ |\phi| \leq \phi_o \end{cases} \tag{5}$$

$$H_z^b(-\underline{u}_z M^o) - H_z^a(\underline{u}_z M^o) = H_z^{sco}, \quad \begin{cases} \rho = a \\ |\phi| \leq \phi_o \end{cases} \tag{6}$$

where $H_z^{sce}$ is the even part of $H_z^{sc}$ and $H_z^{sco}$ is the odd part of $H_z^{sc}$.

Seeking an approximate numerical solution to (5), we let

$$M^e = \sum_{j=1}^{4} V_j^e M_j^e \tag{7}$$

where

$$M_j^e = \begin{cases} \dfrac{(\phi/\phi_o)^{2j-2}}{\sqrt{1 - (\phi/\phi_o)^2}} , & |\phi| \leq \phi \\ 0 , & \text{otherwise} \end{cases} \tag{8}$$

The expansion functions (8) are reasonable because the equivalent magnetic current for a narrow but infinitely long slot in a planar conducting screen of infinite extent excited by a wave TE to the slot axis has $1/\sqrt{w^2 - x^2}$ and $x/\sqrt{w^2 - x^2}$ terms [13, eq. (44)] where w is one half of the slot width and $|x|$ is the distance from the center of the slot. Substitution of (7) into (5) gives

$$\sum_{j=1}^{4} V_j^e [H_z^b(-\underline{u}_z M_j^e) - H_z^a(\underline{u}_z M_j^e)] = H_z^{sce} , \quad \begin{cases} \rho = a \\ |\phi| \leq \phi_o \end{cases} \tag{9}$$

In (9), $H_z^b(-\underline{u}_z M_j^e)$ is the z component of the magnetic field in region a of Fig. 3 and $H_z^a(\underline{u}_z M_j^e)$ is the z component of the magnetic field in region b of Fig. 3. The magnetic fields in Fig. 3 are obtained by solving the boundary value problem in which $E_\phi$, the $\phi$ component of electric field, is continuous at $\rho = a$ where it is given by

$$E_\phi = -M_j^e \tag{10}$$

In terms of the elementary wave functions described in [14, Sec. 5-1],

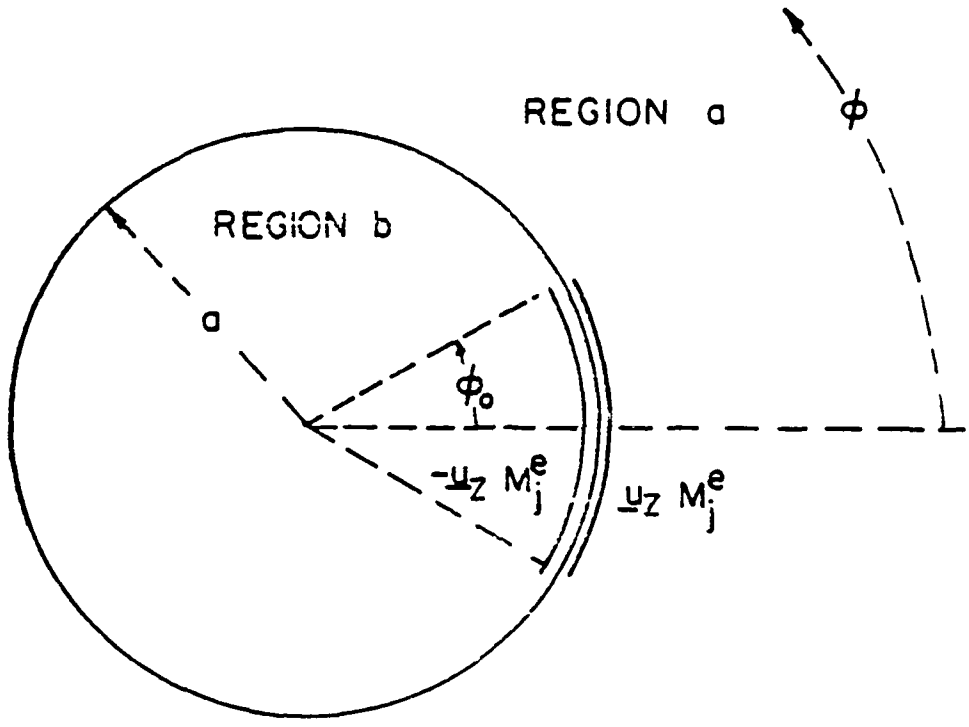


Fig. 3. Situation in which $H_z^a$ and $H_z^b$ of (9) exist.

$$H_z^a(\underline{u}_z M_j^e) = \frac{j}{\eta} \sum_{n=0}^{\infty} \frac{S_{jn}^e H_n^{(2)}(k\rho) \cos(n\phi)}{H_n^{(2)'}(ka)}$$

$$H_z^b(-\underline{u}_z M_j^e) = \frac{j}{\eta} \sum_{n=0}^{\infty} \frac{S_{jn}^e J_n(k\rho) \cos(n\phi)}{J_n'(ka)} \tag{11}$$

where $\eta = \sqrt{\mu/\epsilon}$ and $S_{jn}^e$ is an unknown coefficient. It is evident from [14, eq. (5-19)] that

$$E_\phi = j\eta \frac{\partial H_z}{\partial(k\rho)} \tag{12}$$

where $E_\phi$ is the $\phi$ component of the electric field in Fig. 3 and $H_z$ is the z component of the magnetic field in Fig. 3. Substituting (11) into (12) and using (10), we obtain

$$M_j^e = \sum_{n=0}^{\infty} S_{jn}^e \cos(n\phi) \tag{13}$$

From (13), $S_{jn}^e$ is the Fourier coefficient of $M_j^e$ given by

$$S_{jn}^e = \frac{\epsilon_n}{2\pi} \int_{-\phi_o}^{\phi_o} M_j^e(\phi) \cos(n\phi)\, d\phi \tag{14}$$

Here, $\epsilon_n$ is Neumann's number

$$\epsilon_n = \begin{cases} 1, & n = 0 \\ 2, & n \geq 1 \end{cases} \tag{15}$$

Substitution of (8) into (14) gives

$$S_{jn}^e = \frac{\epsilon_n}{2\pi} \int_{-\phi_o}^{\phi_o} \frac{(\phi/\phi_o)^{2j-2} \cos(n\phi)\, d\phi}{\sqrt{1 - (\phi/\phi_o)^2}} \tag{16}$$

The coefficient $S_{jn}^e$ is evaluated in Appendix A.

Using (11) and the Wronskian [14, eqs. (D-12) and (D-17)]

$$J_n(ka)\, H_n^{(2)'}(ka) - J_n'(ka)\, H_n^{(2)}(ka) = -\frac{2j}{\pi ka} \tag{17}$$

we obtain

$$[H_z^b(-\underline{u}_z \underline{M}_j^e) - H_z^a(\underline{u}_z \underline{M}_j^e)]_{\rho=a} = \frac{2}{\pi\eta ka} \sum_{n=0}^{\infty} \frac{S_{jn}^e \cos(n\phi)}{J_n'(ka)\, H_n^{(2)'}(ka)} \tag{18}$$

which, when substituted into (9), gives

$$\frac{2}{\pi\eta ka} \sum_{j=1}^{4} V_j^e \left( \sum_{n=0}^{\infty} \frac{S_{jn}^e \cos(n\phi)}{J_n'(ka)\, H_n^{(2)'}(ka)} \right) = [H_z^{sce}]_{\rho=a}, \quad |\phi| \leq \phi_o \tag{19}$$

It is evident from [14, eq. (5-116)] that

$$[H_z^{sc}]_{\rho=a} = -\frac{2j}{\pi ka} \sum_{n=-\infty}^{\infty} \frac{j^n e^{jn(\phi-\alpha)}}{H_n^{(2)'}(ka)} \tag{20}$$

The even part of (20) is given by

$$[H_z^{sce}]_{\rho=a} = -\frac{4j}{\pi ka} \sum_{n=0}^{\infty} \frac{\varepsilon_n j^n \cos(n\alpha) \cos(n\phi)}{2H_n^{(2)'}(ka)} \tag{21}$$

Substitution of (21) into (19) and subsequent multiplication by $\pi\eta ka/4$ give

$$\frac{1}{2} \sum_{j=1}^{4} V_j^e \left( \sum_{n=0}^{\infty} \frac{S_{jn}^e \cos(n\phi)}{J_n'(ka)\, H_n^{(2)'}(ka)} \right) = -j\eta \sum_{n=0}^{\infty} \frac{\varepsilon_n j^n \cos(n\alpha) \cos(n\phi)}{2H_n^{(2)'}(ka)}, \quad |\phi| \leq \phi_o \tag{22}$$

Seeking an approximate numerical solution to (6), we let

$$M^o = \sum_{j=1}^{4} V_j^o M_j^o \tag{23}$$

where

$$M_j^o = \begin{cases} \dfrac{(\phi/\phi_o)^{2j-1}}{\sqrt{1-(\phi/\phi_o)^2}}, & |\phi| \le \phi_o \\ 0, & \text{otherwise} \end{cases} \tag{24}$$

Proceeding as in the development (9) - (22), we obtain

$$\frac{1}{2}\sum_{j=1}^{4} V_j^o \left(\sum_{n=1}^{\infty} \frac{S_{jn}^o \sin(n\phi)}{J_n'(ka)\, H_n^{(2)'}(ka)}\right) = -jn \sum_{n=1}^{\infty} \frac{j^n \sin(n\alpha)\sin(n\phi)}{H_n^{(2)'}(ka)}, \quad |\phi| \le \phi_o \tag{25}$$

where

$$S_{jn}^o = \frac{1}{\pi}\int_{-\phi_o}^{\phi_o} \frac{(\phi/\phi_o)^{2j-1}\sin(n\phi)\, d\phi}{\sqrt{1-(\phi/\phi_o)^2}} \tag{26}$$

The coefficient $S_{jn}^o$ is evaluated in Appendix A.

When the frequency is very close to a resonant frequency of the associated cavity, there is an integer p such that $|J_p'(ka)|$ is extremely small. In this case, it can be seen by the following reasoning that any numerical method of solution will fail to accurately determine $V_j^e$. The four cos ($p\phi$) terms on the left-hand side of (22) become so large that none of the other terms can be discerned. As a result, the only informa- that can be extracted from (22) is that

$$\sum_{j=1}^{4} V_j^e S_{jp}^e = 0 \tag{27}$$

This single equation is not sufficient to determine $V_1^e$, $V_2^e$, $V_3^e$, and $V_4^e$.

There should be no difficulty in solving (25) numerically when $|J_o'(ka)|$ is very small because $J_o'(ka)$ does not appear in (25). However,

if $|J_p'(ka)|$ is very small where p is a positive integer, then numerical solution of (25) will be just as difficult as that of (22).

## III. ALTERNATIVE EXPANSION FUNCTIONS

In this section, the expansion functions are changed in order to eliminate the indeterminacy encountered in the last two paragraphs of Section II. If $|J_p'(ka)|$ is extremely small, (7) is replaced by

$$M^e = \sum_{j=1}^{4} \hat{V}_j^e \hat{M}_j^e \tag{28}$$

where

$$\begin{cases} \hat{M}_1^e = J_p'(ka)\, M_1^e \\ \hat{M}_j^e = M_j^e + C_j^e\, M_1^e \ , \quad j=2,3,4 \end{cases} \tag{29}$$

where

$$C_j^e = - S_{jp}^e / S_{1p}^e \tag{30}$$

Comparing (28) with (7) and using (29), we obtain

$$\begin{cases} V_1^e = J_p'(ka)\, \hat{V}_1^e + \sum_{i=2}^{4} C_i^e\, \hat{V}_i^e \\ V_j^e = \hat{V}_j^e \quad , \quad j=2,3,4 \end{cases} \tag{31}$$

In view of (30), substitution of (31) into (22) gives

$$\frac{1}{2}\, \hat{V}_1^e \left( \frac{S_{1p}^e \cos(p\phi)}{H_p^{(2)'}(ka)} + J_p'(ka) \sum_{\substack{n=0 \\ n\neq p}}^{\infty} \frac{S_{1n}^e \cos(n\phi)}{J_n'(ka)\, H_n^{(2)'}(ka)} \right)$$

$$+ \frac{1}{2} \sum_{j=2}^{4} \hat{V}_j^e \left( \sum_{\substack{n=0 \\ n\neq p}}^{\infty} \frac{(S_{jn}^e + C_j^e\, S_{1n}^e) \cos(n\phi)}{J_n'(ka)\, H_n^{(2)'}(ka)} \right)$$

$$= - j\eta \sum_{n=0}^{\infty} \frac{\varepsilon_n j^n \cos(n\alpha) \cos(n\phi)}{2H_n^{(2)'}(ka)}, \quad |\phi| \leq \phi_o \tag{32}$$

Numerical solution of (32) should not be difficult when $|J_p'(ka)|$ is very small because, in contrast to (22), (32) does not contain any huge $\cos(p\phi)$ terms which obscure all the other terms.

If $|J_o'(ka)|$ is very small, (25) is retained. However, if $|J_p'(ka)|$ is very small where p is a positive integer, then (23) is replaced by

$$M^o = \sum_{j=1}^{4} \hat{V}_j^o \hat{M}_j^o \tag{33}$$

where

$$\begin{cases} \hat{M}_1^o = J_p'(ka)\, M_1^o \\ \hat{M}_j^o = M_j^o + C_j^o M_1^o, \quad j=2,3,4 \end{cases} \tag{34}$$

where

$$C_j^o = - S_{jp}^o / S_{1p}^o \tag{35}$$

Comparing (33) with (23) and using (34), we obtain

$$\begin{cases} V_1^o = J_p'(ka)\, \hat{V}_1^o + \sum_{i=2}^{4} C_i^o \hat{V}_i^o \\ V_j^o = \hat{V}_j, \quad j=2,3,4 \end{cases} \tag{36}$$

In view of (35), (36) causes (25) to be replaced by

$$\frac{1}{2} \hat{V}_1^o \left( \frac{S_{1p}^o \sin(p\phi)}{H_p^{(2)'}(ka)} + J_p'(ka) \sum_{\substack{n=1 \\ n\neq p}}^{\infty} \frac{S_{1n}^o \sin(n\phi)}{J_n'(ka)\, H_n^{(2)'}(ka)} \right)$$

$$+ \frac{1}{2} \sum_{j=2}^{4} \hat{V}_j^o \left( \sum_{\substack{n=1 \\ n\neq p}}^{\infty} \frac{(S_{jn}^o + C_j^o S_{1n}^o) \sin(n\phi)}{J_n'(ka)\, H_n^{(2)'}(ka)} \right)$$

$$= - j\eta \sum_{n=1}^{\infty} \frac{j^n \sin(n\alpha) \sin(n\phi)}{H_n^{(2)'}(ka)}, \quad |\phi| \leq \phi_o \tag{37}$$

Equation (37) is valid for $p \geq 1$. If $p = 0$, we revert to (25). Numerical solution of (37) should not be difficult when $|J_p'(ka)|$ is very small because, in contrast to (25), (37) does not contain any huge sin $(p\phi)$ terms which obscure all the other terms.

Equations (5) and (6) can be viewed as operator equations. For example, (5) is

$$L\, M^e = g \tag{38}$$

where L is an operator and g is a known function. Now, (18) is $LM_j^e$ where $M_j^e$ is given by (13). Since (8) was not used in its derivation, (18) can be generalized to mean that, given an even $2\pi$ periodic but otherwise arbitrary function $f(\phi)$, Lf is the right-hand side of (18) where $\{S_{jn}^e\}$ are the Fourier coefficients of f. Taking $f = \cos(p\phi)$, we obtain

$$L(\cos(p\phi)) = \frac{2\cos(p\phi)}{\pi\eta ka\, J_p'(ka)\, H_p^{(2)'}(ka)} \tag{39}$$

When $|J_p'(ka)|$ is very small, the expansion functions $\{M_j^e,\ j=1,2,3,4\}$ are not good because each one of them contains $\cos(p\phi)$ so that all of the functions $\{L(M_j^e),\ j=1,2,3,4\}$, being roughly proportional to $\cos(p\phi)$, are nearly indistinguishable from each other. The expansion functions $\{\hat{M}_j^e,\ j=1,2,3,4\}$ are better because $\hat{M}_1^e$, which contains $\cos(p\phi)$, is normalized so that $L\hat{M}_1^e$ remains finite, and none of the functions $\{\hat{M}_j^e,\ j=2,3,4\}$ contains $\cos(p\phi)$. Therefore, none of the functions $\{L\hat{M}_j^e,\ j=2,3,4\}$ contains $\cos(p\phi)$. Since none of them are dominated by $\cos(p\phi)$, the functions $\{L\hat{M}_j^e,\ j=2,3,4\}$ are easily distinguishable from each other and from $L\hat{M}_1^e$.

## IV. TESTING FUNCTIONS

In this section, 4 linear equations are extracted from the functional equation (32) by multiplying (32) by each of 4 even functions called testing functions and integrating from $-\phi_o$ to $\phi_o$ with respect to $\phi$. Similarly, four linear equations are extracted from (37) by multiplying (37) by each of four odd testing functions and integrating over the slot.

Called $\{W_i^e,\ i=1,2,3,4\}$, the even testing functions are defined by

$$W_i^e = (\phi/\phi_o)^{2i-2}, \quad i=1,2,3,4 \tag{40}$$

Multiplying (32) by $W_i^e$ and integrating over the slot, we obtain four equations, one for each value of i. In matrix notation, these equations are

$$Y^e \vec{\hat{V}}^e = \vec{I}^e \tag{41}$$

where $\vec{\hat{V}}^e$ is the column vector whose jth element is $\hat{V}_j^e$ and $Y^e$ is the $4 \times 4$ matrix whose elements are given by

$$Y_{i1}^e = \frac{F_{ip}^e\ S_{1p}^e}{H_p^{(2)'}(ka)} + J_p'(ka) \sum_{\substack{n=0 \\ n\neq p}}^{\infty} \frac{F_{in}^e\ S_{1n}^e}{J_n'(ka)\ H_n^{(2)'}(ka)}, \quad i=1,2,3,4 \tag{42}$$

$$Y_{ij}^e = \sum_{\substack{n=0 \\ n\neq p}}^{\infty} \frac{F_{in}^e (S_{jn}^e + C_j^e\ S_{1n}^e)}{J_n'(ka)\ H_n^{(2)'}(ka)}, \quad \begin{cases} i = 1,2,3,4 \\ j = 2,3,4 \end{cases} \tag{43}$$

where

$$F_{in}^e = \frac{1}{2} \int_{-\phi_o}^{\phi_o} (\phi/\phi_o)^{2i-2} \cos(n\phi)\, d\phi \tag{44}$$

The coefficient $F_{in}^e$ is evaluated in [11, Appendix B]. In (41), $\vec{I}^e$ is the column vector whose elements are given by

$$I_i^e = -2jn \sum_{n=0}^{\infty} \frac{\varepsilon_n j^n F_{in}^e \cos(n\alpha)}{2H_n^{(2)'}(ka)}, \quad i=1,2,3,4 \tag{45}$$

The odd testing functions are defined by

$$W_i^o = (\phi/\phi_o)^{2i-1} , \quad i = 1,2,3,4 \tag{46}$$

We multiply (37) by $W_i^o$ and integrate over the slot. Doing this for i=1,2,3, and 4, we obtain the matrix equation

$$Y^o \vec{\hat{V}}^o = \vec{I}^o \tag{47}$$

where $\vec{\hat{V}}^o$ is the column vector whose jth element is $\hat{V}_j^o$, and $Y^o$ is the $4 \times 4$ matrix whose elements are given by

$$Y_{il}^o = \frac{F_{ip}^o \, S_{lp}^o}{H_p^{(2)'}(ka)} + J_p'(ka) \sum_{\substack{n=1 \\ n \neq p}}^{\infty} \frac{F_{in}^o \, S_{ln}^o}{J_n'(ka) \, H_n^{(2)'}(ka)} , \quad i=1,2,3,4 \tag{48}$$

$$Y_{ij}^o = \sum_{\substack{n=1 \\ n \neq p}}^{\infty} \frac{F_{in}^o (S_{jn}^o + C_j^o \, S_{ln}^o)}{J_n'(ka) \, H_n^{(2)'}(ka)} , \qquad \begin{cases} i = 1,2,3,4 \\ j = 2,3,4 \end{cases} \tag{49}$$

where

$$F_{in}^o = \frac{1}{2} \int_{-\phi_o}^{\phi_o} (\phi/\phi_o)^{2i-1} \sin(n\phi) \, d\phi \tag{50}$$

The coefficient $F_{in}^o$ is evaluated in [11, Appendix B]. In (47) $\vec{I}^o$ is the column vector whose elements are given by

$$I_i^o = -2jn \sum_{n=1}^{\infty} \frac{j^n \, F_{in}^o \sin(n\alpha)}{H_n^{(2)'}(ka)} , \quad i = 1,2,3,4 \tag{51}$$

Actually, (47)-(49) are valid only for $p > 0$. For $p = 0$, we multiply (25) by $W_i^o$ and integrate over the slot. Doing this for $i = 1,2,3$, and 4, we obtain (47) with the elements of $\vec{\hat{V}}^o$ given by

$$\hat{V}_j^o = V_j^o , \tag{52}$$

with the elements of $Y^o$ given by

$$Y^o_{ij} = \sum_{n=1}^{\infty} \frac{F^o_{in}\, S^o_{jn}}{J'_n(ka)\, H^{(2)'}_n(ka)} \quad , \tag{53}$$

and with the elements of $\vec{I}^o$ given by (51).

After (41) is solved for $\vec{V}^e$, $M^e$ will be given by (7) with $\{V^e_j,\ j=1,2,3,4\}$ given by (31). After (47) is solved for $\vec{V}^o$, $M^o$ will be given by (23) with $\{V^o_j,\ j = 1,2,3,4\}$ given by (36) for $p \neq 0$ and, according to (52), by

$$V^o_j = \hat{V}^o_j \ , \quad j = 1,2,3,4 \tag{54}$$

for $p = 0$. Finally, $\underline{M}$ is given by (4) where $M^e$ and $M^o$ have been described in the previous two sentences:

$$\underline{M} = \underline{u}_z \sum_{j=1}^{4} (V^e_j M^e_j + V^o_j M^o_j) \tag{55}$$

The magnetic field in Fig. 2 is $\underline{u}_z H_z$ where

$$H_z = \begin{cases} H^a_z(\underline{M}) + H^{sc}_z \ , & \rho > a \\ H^b_z(-\underline{M}) \ , & \rho < a \end{cases} \tag{56}$$

where $H^{sc}_z$, $H^a_z(\underline{M})$, and $H^b_z(-\underline{M})$ are the z components of the magnetic fields due to the incident wave, $\underline{M}$, and -M, respectively. From (1) and [14, eqs. (5-114) and (5-115)], we obtain

$$H^{sc}_z = \sum_{n=0}^{\infty} \epsilon_n j^n [J_n(k\rho) - \frac{J'_n(ka)}{H^{(2)'}_n(ka)} H^{(2)}_n(k\rho)] \cos(n(\phi-\alpha)) \tag{57}$$

From (55), we have

$$\begin{cases} H_z^a(\underline{M}) = \sum_{j=1}^{4} (V_j^e H_z^a(\underline{u}_z M_j^e) + V_j^o H_z^a(\underline{u}_z M_j^o)) \\ H_z^b(-\underline{M}) = \sum_{j=1}^{4} (V_j^e H_z^b(-\underline{u}_z M_j^e) + V_j^o H_z^b(-\underline{u}_z M_j^o)) \end{cases} \tag{58}$$

where $H_z^a(\underline{u}_z M_j^e)$ and $H_z^b(-\underline{u}_z M_j^e)$ are given by (11). Similarly,

$$\begin{cases} H_z^a(\underline{u}_z M_j^o) = \frac{j}{\eta} \sum_{n=1}^{\infty} \frac{S_{jn}^o H_n^{(2)}(k\rho) \sin(n\phi)}{H_n^{(2)'}(ka)} \\ H_z^b(-\underline{u}_z M_j^o) = \frac{j}{\eta} \sum_{n=1}^{\infty} \frac{S_{jn}^o J_n(k\rho) \sin(n\phi)}{J_n'(ka)} \end{cases} \tag{59}$$

so that (58) expands to

$$H_z^a(\underline{M}) = \frac{j}{\eta} \left[ \sum_{j=1}^{4} V_j^e \left( \sum_{n=0}^{\infty} \frac{S_{jn}^e H_n^{(2)}(k\rho) \cos(n\phi)}{H_n^{(2)'}(ka)} \right) + \sum_{j=1}^{4} V_j^o \left( \sum_{n=1}^{\infty} \frac{S_{jn}^o H_n^{(2)}(k\rho) \sin(n\phi)}{H_n^{(2)'}(ka)} \right) \right] \tag{60}$$

$$H_z^b(-\underline{M}) = \frac{j}{\eta} \left[ \sum_{j=1}^{4} V_j^e \left( \sum_{\substack{n=0 \\ n\neq p}}^{\infty} \frac{S_{jn}^e J_n(k\rho) \cos(n\phi)}{J_n'(ka)} \right) + B_p^e J_p(k\rho) \cos(p\phi) \right.$$

$$\left. + \sum_{j=1}^{4} V_j^o \left( \sum_{\substack{n=1 \\ n\neq p}}^{\infty} \frac{S_{jn}^o J_n(k\rho) \sin(n\phi)}{J_n'(ka)} \right) + B_p^o J_p(k\rho) \sin(p\phi) \right] \tag{61}$$

where

$$B_p^e = \frac{1}{J_p'(ka)} \sum_{j=1}^{4} V_j^e S_{jp}^e \tag{62}$$

$$B_p^o = \frac{1}{J_p'(ka)} \sum_{j=1}^{4} V_j^o S_{jp}^o \tag{63}$$

If $p = 0$, the $B_p^o$ term is to be omitted from (61).

Do $B_p^e$ and $B_p^o$ remain finite as $J_p'(ka)$ approaches zero? In view of (30), substitution of (31) into (62) gives

$$B_p^e = S_{1p}^e \hat{V}_1^e \tag{64}$$

Substituting (36) into (63) and using (35), we obtain

$$B_p^o = S_{1p}^o \hat{V}_1^o , \quad p \neq 0 \tag{65}$$

As given by (64) and (65), $B_p^e$ and $B_p^o$ remain finite as $J_p'(ka)$ approach zero.

When $\rho = 0$, (61) reduces to

$$H_z^b(-\underline{M}) = \begin{cases} \frac{j}{\eta} \hat{V}_1^e S_{10}^e & , \ p = 0 \\ \frac{j}{\eta J_o'(ka)} \sum_{j=1}^{4} V_j^e S_{j0}^e & , \ p \neq 0 \end{cases} \tag{66}$$

Equation (66) was obtained by using (64) and [14, eqs. (D-9) and (D-10)]

$$J_n(0) = \begin{cases} 1 , & n = 0 \\ 0 , & n \geq 1 \end{cases} \tag{67}$$

In the preceding three paragraphs, we found $\underline{u}_z H_z$, the magnetic field in Fig. 2. Called $\underline{E}$, the electric field in Fig. 2 is given by [14, eq. (5-19)]

$$\underline{E} = - \frac{j\eta}{k} (\nabla H_z \times \underline{u}_z) \tag{68}$$

Since $\underline{M}$ was determined such that the situation in Fig. 2 is equivalent to that in Fig. 1, the fields in Fig. 2 are the same as those in Fig. 1. Thus, we have obtained our objective, which was to find the fields everywhere in Fig. 1.

## V. BISTATIC SCATTERING WIDTH

The bistatic scattering width is called $\sigma$ and is defined by [15, eq. (3-49)]

$$\sigma = \lim_{\rho\to\infty} \left(2\pi\rho\left|\frac{H_z^s}{H_z^i}\right|^2\right) \tag{69}$$

where $H_z^i$ is the z component of the incident magnetic field given by (1) and $H_z^s$ is the z component of the scattered magnetic field given by

$$H_z^s = H_z - H_z^i \tag{70}$$

where $H_z$ is the total magnetic field given by (56). Substitution of (56) into (70) gives

$$H_z^s = H_z^a(\underline{M}) + H_z^{sc} - H_z^i \ , \quad \rho > a \tag{71}$$

It is evident from (1) and [14, eq. (5-113)] that

$$H_z^i = \sum_{n=0}^{\infty} \varepsilon_n j^n J_n(k\rho) \cos\,(n(\phi-\alpha)) \tag{72}$$

Subtracting (72) from (57), we obtain

$$H_z^{sc} - H_z^i = - \sum_{n=0}^{\infty} \frac{\varepsilon_n j^n J_n'(ka)\, H_n^{(2)}(k\rho) \cos\,(n(\phi-\alpha))}{H_n^{(2)'}(ka)} \tag{73}$$

Substitution of (60) and (73) into (71) gives

$$H_z^s = \sum_{n=0}^{\infty} \left[\frac{j}{\eta}\left(\sum_{j=1}^{4} V_j^e S_{jn}^e\right) - \varepsilon_n j^n J_n'(ka) \cos\,(n\alpha)\right] \frac{H_n^{(2)}(k\rho) \cos\,(n\phi)}{H_n^{(2)'}(ka)}$$

$$+ \sum_{n=1}^{\infty} \left[\frac{j}{\eta}\left(\sum_{j=1}^{4} V_j^o S_{jn}^o\right) - 2j^n J_n'(ka) \sin\,(n\alpha)\right] \frac{H_n^{(2)}(k\rho) \sin\,(n\phi)}{H_n^{(2)'}(ka)} \tag{74}$$

Substituting (74) into (69), recognizing that $|H_z^i| = 1$, using the large argument formula [14, eq. (D-13)]

$$H_n^{(2)}(k\rho) \approx \sqrt{\frac{2j}{\pi k\rho}}\, j^n\, e^{-jk\rho}\ , \tag{75}$$

and dividing both sides of (69) by $\pi a$, we obtain

$$\frac{\sigma}{\pi a} = \frac{4}{\pi ka}\Bigg|\sum_{n=0}^{\infty}\left[\frac{j^{n+1}}{\eta}\left(\sum_{j=1}^{4} V_j^e S_{jn}^e\right) - \varepsilon_n(-1)^n J_n'(ka)\cos(n\alpha)\right]\frac{\cos(n\phi)}{H_n^{(2)'}(ka)}$$

$$+\sum_{n=1}^{\infty}\left[\frac{j^{n+1}}{\eta}\left(\sum_{j=1}^{4} V_j^o S_{jn}^o\right) - 2(-1)^n J_n'(ka)\sin(n\alpha)\right]\frac{\sin(n\phi)}{H_n^{(2)'}(ka)}\Bigg|^2 \tag{76}$$

If there were no slit, then $\{V_j^e = V_j^o = 0,\ j=1,2,3,4\}$ and (76) would reduce to a quantity called $\sigma^{sc}/\pi a$:

$$\frac{\sigma^{sc}}{\pi a} = \frac{4}{\pi ka}\left|\sum_{n=0}^{\infty}\frac{(-1)^n\varepsilon_n J_n'(ka)\cos(n(\phi-\alpha))}{H_n^{(2)'}(ka)}\right|^2 \tag{77}$$

The quantity $\sigma^{sc}/\pi a$ is the normalized bistatic scattering width of the closed cylinder, i.e., the short-circuit normalized bistatic scattering width. This width is that associated with the well-known scattering pattern [14, eq. (5-117)] of the closed cylinder.

## VI. NARROW SLOT AT RESONANCE

If the slot aperture is narrow and if the associated cavity is resonant, that is, if there is a non-negative integer p such that $J_p'(ka) = 0$, then we can show that the slit cylinder scatters nearly the same as the corresponding closed cylinder and we can find approximate expressions for the field components inside the cylinder. Thus, we will

have values against which we can check field components and bistatic scattering widths computed from formulas in Sections IV and V.

In order to do what is proposed in the first sentence of this section, we consider

$$\underline{J} = \underline{J}^{sc} + \underline{J}^{A} \tag{78}$$

where $\underline{J}^{sc}$ is the electric current that would be induced on the corresponding closed cylinder:

$$\underline{J}^{sc} = - \underline{u}_{\phi} [H_z^{sc}]_{\rho=a} \tag{79}$$

Moreover, $\underline{J}^{A}$ is the electric current at $\rho = a$ given by

$$\underline{J}^{A} = \underline{u}_{\phi}(A_p^e \cos (p\phi) + A_p^o \sin (p\phi)) \tag{80}$$

where $A_p^e$ and $A_p^o$ are constants. In (79) and (80), $\underline{u}_{\phi}$ is the unit vector in the $\phi$ direction. The z component of magnetic field, $H_z^A$, and the $\phi$ component of electric field, $E_{\phi}^A$, produced by $\underline{J}^{A}$ radiating in the homogeneous medium with constitutive parameters $\mu$ and $\varepsilon$ are given by

$$H_z^A = \begin{cases} \dfrac{J_p(k\rho)}{J_p(ka)} (A_p^e \cos (p\phi) + A_p^o \sin (p\phi)) & , \ \rho < a \\ 0 & , \ \rho > a \end{cases} \tag{81}$$

$$E_{\phi}^A/\eta = \begin{cases} \dfrac{j\, J_p'(k\rho)}{J_p(ka)} (A_p^e \cos (p\phi) + A_p^o \sin (p\phi)) & , \ \rho \leq a \\ 0 & , \ \rho \geq a \end{cases} \tag{82}$$

The $\rho$ component of electric field produced by $\underline{J}^{A}$ is not considered here.

Since $E_{\phi}^A/\eta$ vanishes at $\rho = a$, the $\phi$ directed electric field produced by $\underline{J}$ of (78) cancels the $\phi$ directed incident electric field

at $\rho = a$, Thus, if it did not spill over into the aperture, $\underline{J}$ would be the true electric current induced on the slotted cylindrical surface. Now, if $A_p^e$ and $A_p^o$ are adjusted so that both $J_\phi$ and $\frac{dJ_\phi}{d\phi}$ vanish at $\phi = 0$, then $\underline{J}$ will be small in the aperture and therefore will be a good approximation to the true electric current. Here, $J_\phi$ is the $\phi$ component of $\underline{J}$. Actually, if $p = 0$, then $A_p^o$ drops out of $\underline{J}$ and only $J_\phi$ can be made to vanish at $\phi = 0$. Substituting (79) and (80) into (78), using (20), and forcing $J_\phi$ and $\frac{dJ_\phi}{d\phi}$ to vanish at $\phi = 0$, we obtain

$$A_p^e = -\frac{4j}{\pi ka} \sum_{n=0}^{\infty} \frac{\varepsilon_n j^n \cos(n\alpha)}{2H_n^{(2)'}(ka)} \tag{83}$$

$$A_p^o = -\frac{4j}{p\pi ka} \sum_{n=1}^{\infty} \frac{n j^n \sin(n\alpha)}{H_n^{(2)'}(ka)}, \quad p \neq 0 \tag{84}$$

In the preceding paragraph, we found that the electric current on the slit cylinder is approximately $\underline{J}$ of (78)-(80) with $A_p^e$ and $A_p^o$ given by (83) and (84) if the slit is narrow and if the associated cavity is resonant. Thus, the field that exists in the presence of the slit cylinder is approximately the field which would exist in the presence of the associated closed cylinder plus the field produced by $\underline{J}^A$. Since there is no field inside the associated closed cylinder, the field inside the slit cylinder is approximately the field due to $\underline{J}^A$. Substituting (83) and (84) into (81) and (82) and using [14, eq. (D-17)] and the fact that $J_p'(ka) = 0$, we express the components (81) and (82) of this interior field due to $\underline{J}^A$ as

$$H_z^A = -2jY_p'(ka)J_p(k\rho)\left[\left(\sum_{n=0}^{\infty}\frac{\varepsilon_n j^n \cos(n\alpha)}{2H_n^{(2)'}(ka)}\right)\cos(p\phi)+\frac{1}{p}\left(\sum_{n=1}^{\infty}\frac{nj^n\sin(n\alpha)}{H_n^{(2)'}(ka)}\right)\sin(p\phi)\right] \tag{85}$$

$$E_\phi^A/\eta = 2Y_p'(ka)J_p'(k\rho)\left[\left(\sum_{n=0}^{\infty}\frac{\varepsilon_n j^n\cos(n\alpha)}{2H_n^{(2)'}(ka)}\right)\cos(p\phi)+\frac{1}{p}\left(\sum_{n=1}^{\infty}\frac{nj^n\sin(n\alpha)}{H_n^{(2)'}(ka)}\right)\sin(p\phi)\right] \tag{86}$$

where the 1/p terms are to be discarded if p=0. Here, $Y_p(ka)$ is the Bessel function of the second kind of order p. The field components (85) and (86) are approximately those inside the slit cylinder when the slit is narrow and the associated cavity is resonant. Since, according to (81) and (82), the field due to $\underline{J}^A$ vanishes outside the cylinder, we deduce that the field outside this slit cylinder is approximately the field that would exist outside the corresponding closed cylinder.

In the preceding paragraph, we have shown that, if the slit is narrow and if the corresponding closed cylinder is resonant, then the field components inside the slit cylinder are approximately (85) and (86) and the field outside the cylinder is approximately the field which would exist if there were no slit. Since neither (85) nor (86) depend on the width of the slit, it is evident that the amount of TE field that enters a resonant circular cylindrical cavity through an infinitely long but narrow slit does not depend on the width of the slit.

## VII. NUMERICAL RESULTS AND DISCUSSION

By means of a computer program that will be described in a forthcoming report, $|E_\phi/\eta|$ of (68) was calculated in the aperture, and $|E_\phi/\eta|$ of (68) and $|H_z|$ of (56) were calculated at the center of the aperture and at the center of the cylinder. The normalized scattering

widths $\sigma/\pi a$ of (76) and $\sigma^{sc}/\pi a$ of (77) were also calculated at $(\phi,\alpha)$ = (0°, 0°), (180°, 0°), and (180°, 180°). Results of these calculations obtained by truncating the summations with respect to n at n = 10,000 are presented here.

The aperture field amplitude $|E_\phi/\eta|$ shown in Fig. 4 agrees well with [1, Fig. 27] and [16, Fig. 11]. The data of Fig. 4 were obtained by replacing (7) by

$$M^e = \sum_{j=1}^{NN} V_j^e M_j^e \quad , \quad NN \leq 4 \tag{87}$$

If NN < 4, the matrix $Y^e$ and the column vectors $\vec{V}^e$ and $\vec{I}^e$ in (41) were truncated accordingly. In Fig. 4, the aperture field amplitude obtained by using NN = 1 is nearly the same as that obtained by using NN = 4. However, the field amplitude obtained by using NN = 1 is very different from that obtained by using NN = 4 in the wider slit aperture of Fig. 5. Nevertheless, the field amplitude obtained by using NN = 3 in Fig. 5 is nearly the same as that obtained by using NN = 4. The curve for which NN = 4 in Fig. 5 agrees with [2, Fig. 4].

Figure 6 shows a ka scan of $|E_\phi/\eta|$ at the center ($\rho$=a, $\phi$=0) of the slit aperture in the cylinder of Fig. 1 for $\phi_o$ = 5° and $\alpha$ = 0°. The data of Fig. 6 and of all subsequent figures were obtained by using NN = 4. In Fig. 7, the data of Fig. 6 are plotted on a logarithmic scale. The peak of $|E_\phi/\eta|$ at ka = 0.374 is probably due to the H-pol low frequency resonance noted in [8, p. 519]. The three minima of $|E_\phi/\eta|$ occur very close to resonant values of ka. Resonant values of ka are values of ka for which there is a non-negative integer p such that $J_p'(ka) = 0$. After dipping to a minimum very close to a resonant value

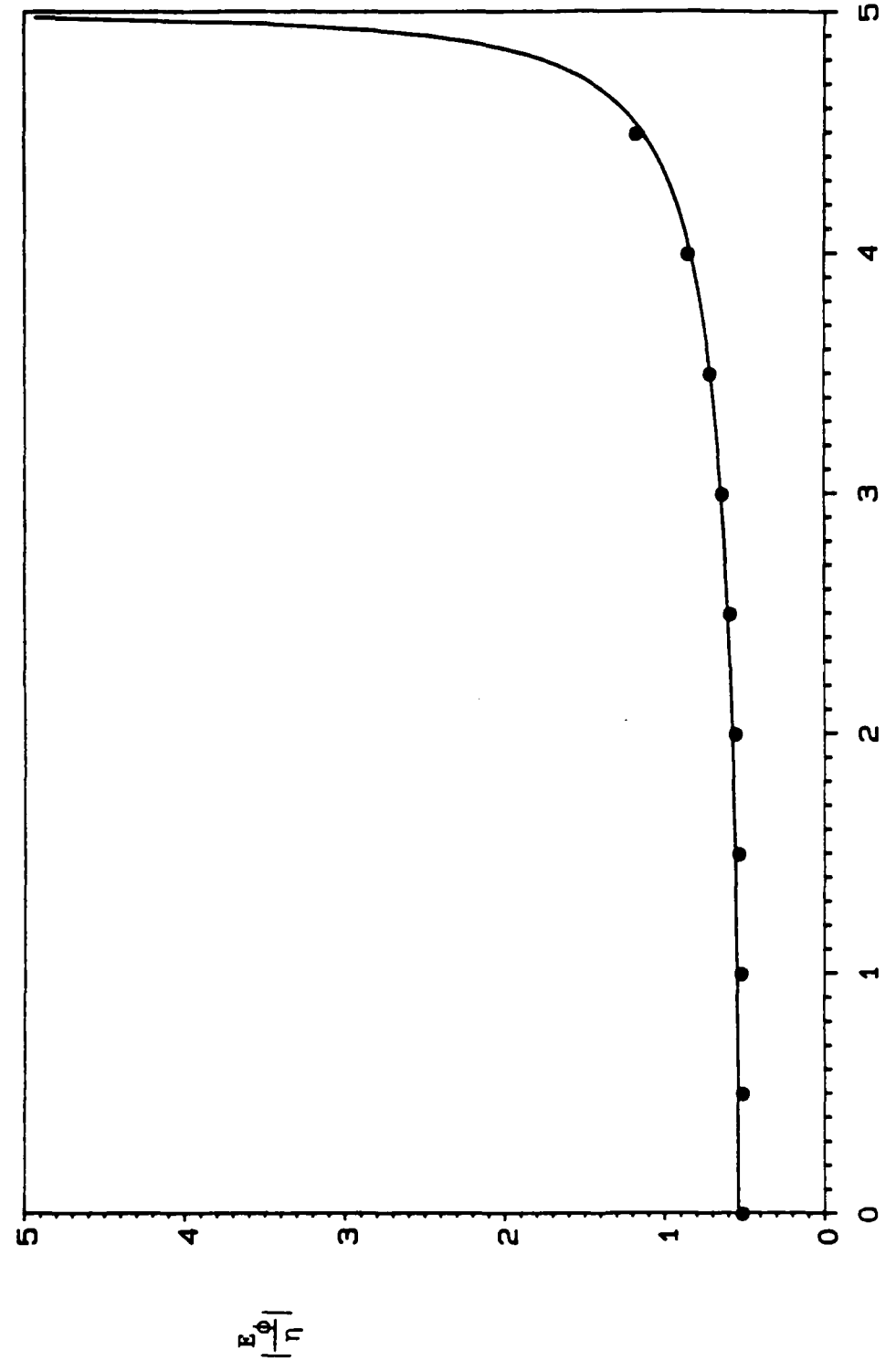


Fig. 4. Field amplitude $\left|\frac{E_\phi}{\eta}\right|$ in the aperture for $\phi_o = 5°$, $\alpha = 180°$, and $ka = 3.456$. Since $\alpha = 180°$, the slit aperture is in the shadow region. The solid curve is the solution for which NN = 4. The symbol ⊕ represents the solution for which NN = 1.

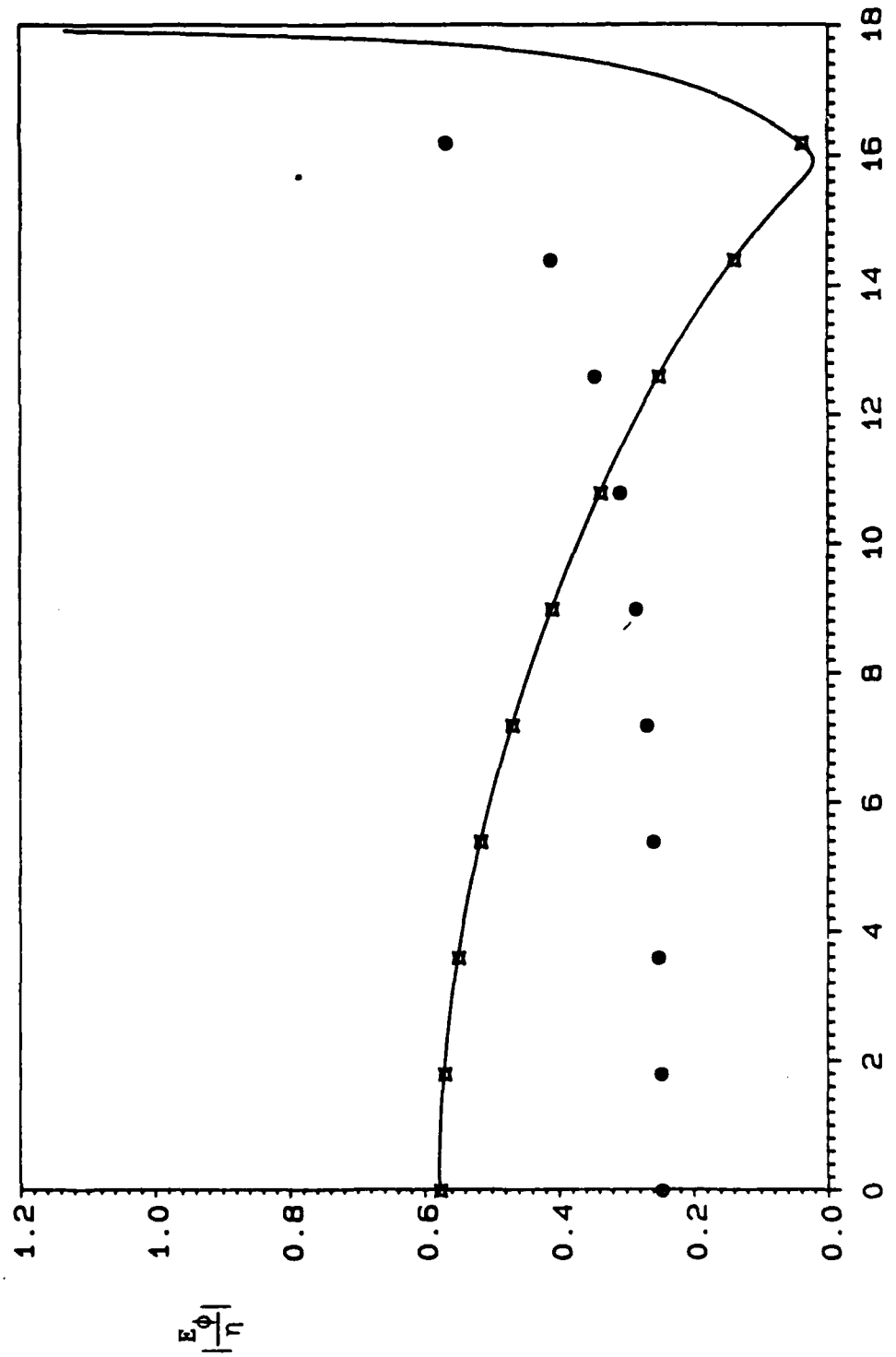


Fig. 5. Field amplitude $\left|\frac{E_\phi}{\eta}\right|$ in the aperture for $\phi_o = 18°$, $\alpha = 0°$, and ka = 10. Since $\alpha = 0°$, the slit aperture is in the illumination region. The solid curve is the solution for which NN = 4. The symbols $\oplus$ and $\square$ represent the solutions for which NN = 1 and NN = 3, respectively.

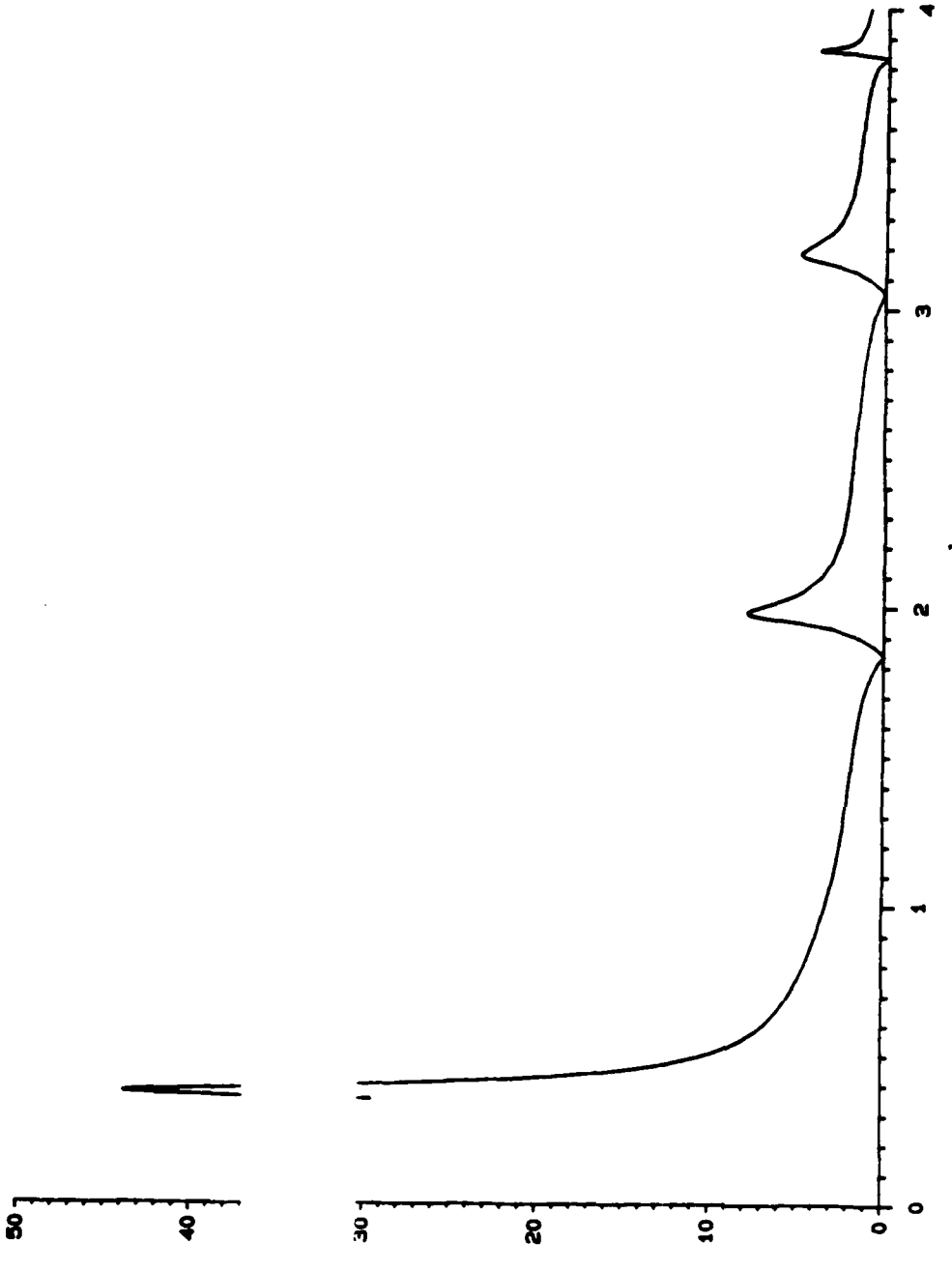


Fig. 6. Field amplitude $|\frac{E_\phi}{\eta}|$ at the center of the aperture for $\phi_o = 5°$ and $\alpha = 0°$.

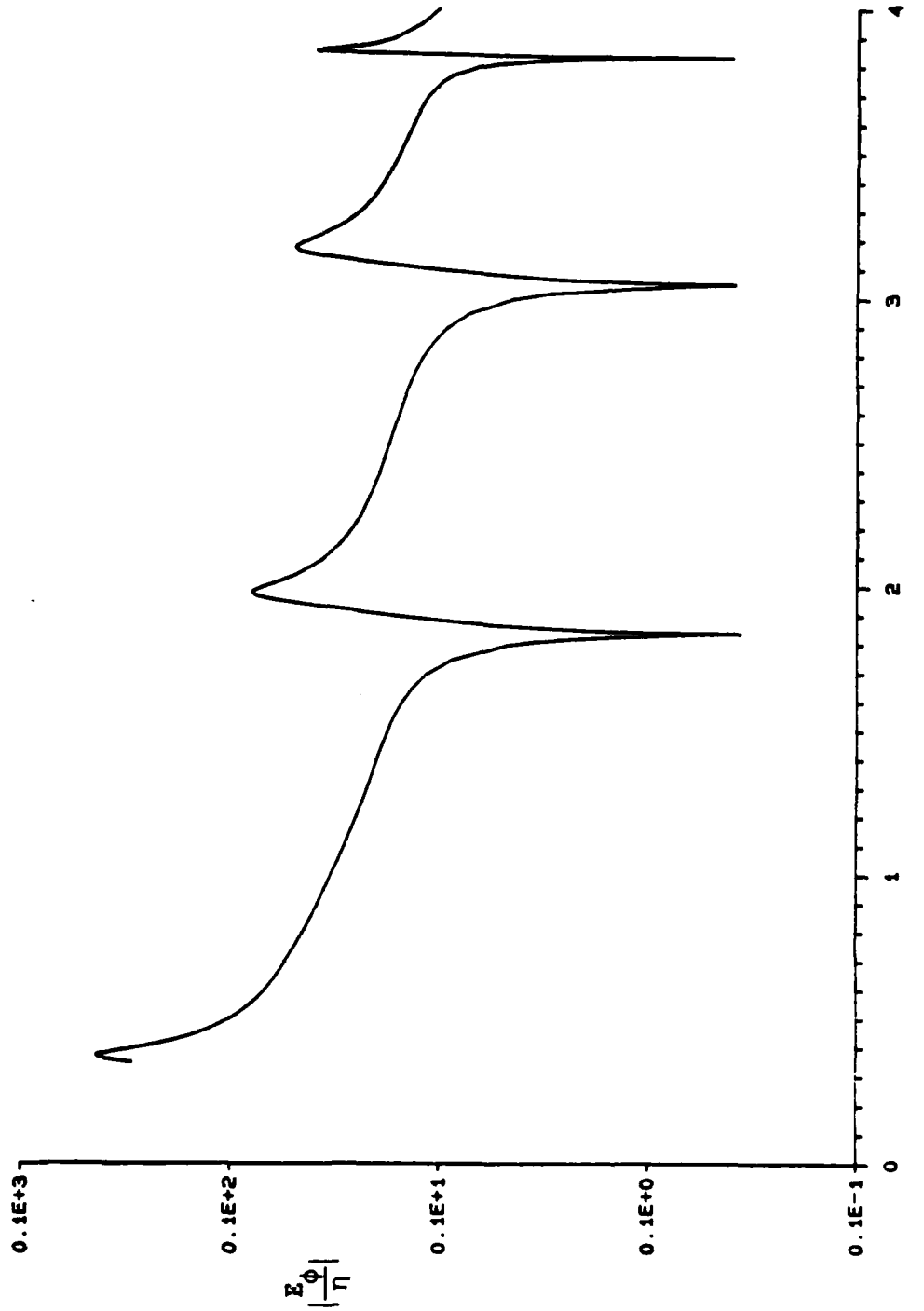


Fig. 7. Field amplitude $\left|\frac{E_\phi}{\eta}\right|$ at the center of the aperture for $\phi_o = 5°$ and $\alpha = 0°$ plotted on a logarithmic scale.

of ka, $|E_\phi/\eta$ ises sharply tc imum at a larger va a.
According to cussion in Sect , $|E_\phi/\eta|$ should app ro
at resonant \ f ka as the wid he aperture approa o.
The values of at the first s nant values of ka lated
in Table 1. alues of $|E_\phi/\eta|$ t exactly minimum For
instance, the ed value of $|E_\phi$ its first minimum 6
rather than (

Figu ws $|H_z|$ at the of the aperture in inder
of Fig. 6. 9, the data of are plotted on a l ic
scale. Table s $|H_z|$ at the f ix resonant values The
corresponding aperture result | of (85) are also r
comparison. nt is excellent

Figu ows $|E_\phi/\eta|_o$ at ter of the slit cy f
Fig. 6. The pt "o" on $|E_\phi/$ notes evaluation at
In Fig. 11, t of Fig. 10 are d on a logarithmic
Table 2 shows $_o$ and the corre g small aperture r
$|E_\phi^A/\eta|_o$ of (8 he first six re values of ka. In
$|E_\phi/\eta|_o$ is sn n $|E_\phi^A/\eta|_o = 0$ . I more $|E_\phi/\eta|_o$ agree ith
$|E_\phi^A/\eta|_o$ at th sonant values here $|E_\phi^A/\eta|_o \neq 0$.

Figu ows $|H_z|$ at the r of the slit cylin ig. 6.
In Fig. 13, t of Fig. 12 are d on a logarithmic
Table 2 shows nd the correspo small aperture resu of
(85) at the f x resonant valu ka. In Table 2, |H all
when $|H_z^A|$ = ( close agreement $_z|$ with $|H_z^A|$ at ka 706
is remarkable e, as observed . 12, the curve of sus
ka is very st ka = 3.831706.

Table 1. Field amplitudes $|E_\phi/\eta|$ and $|H_z|$ at the center of the aperture for resonant values of ka. $\phi_o = 5°$ and $\alpha = 0°$. For comparison, $|E_\phi^A/\eta|$ of (86) and $|H_z^A|$ of (85) are also tabulated.

| ka | $\lvert E_\phi/\eta\rvert$ | $\lvert E_\phi^A/\eta\rvert$ | $\lvert H_z\rvert$ | $\lvert H_z^A\rvert$ |
|---|---|---|---|---|
| 1.841184 | 0.039 | 0.0 | 1.867 | 1.866 |
| 3.054237 | 0.065 | 0.0 | 1.921 | 1.914 |
| 3.831706 | 0.040 | 0.0 | 1.944 | 1.945 |
| 4.20119 | 0.098 | 0.0 | 1.954 | 1.938 |
| 5.31755 | 0.132 | 0.0 | 1.983 | 1.954 |
| 5.33144 | 0.042 | 0.0 | 1.955 | 1.953 |

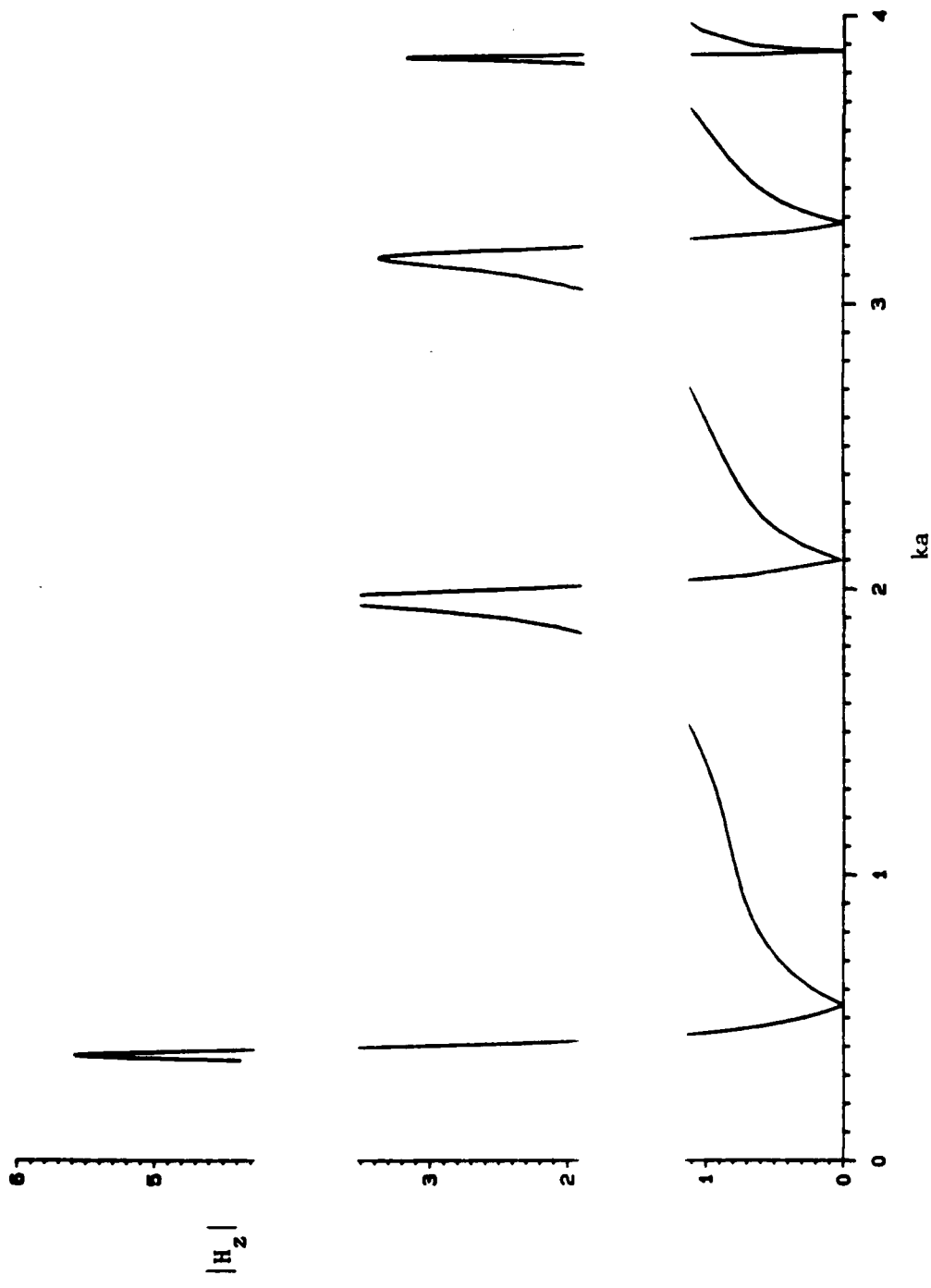


Fig. 8. Field amplitude $|H_z|$ at the center of the aperture for $\phi_o = 5°$ and $\alpha = 0°$.

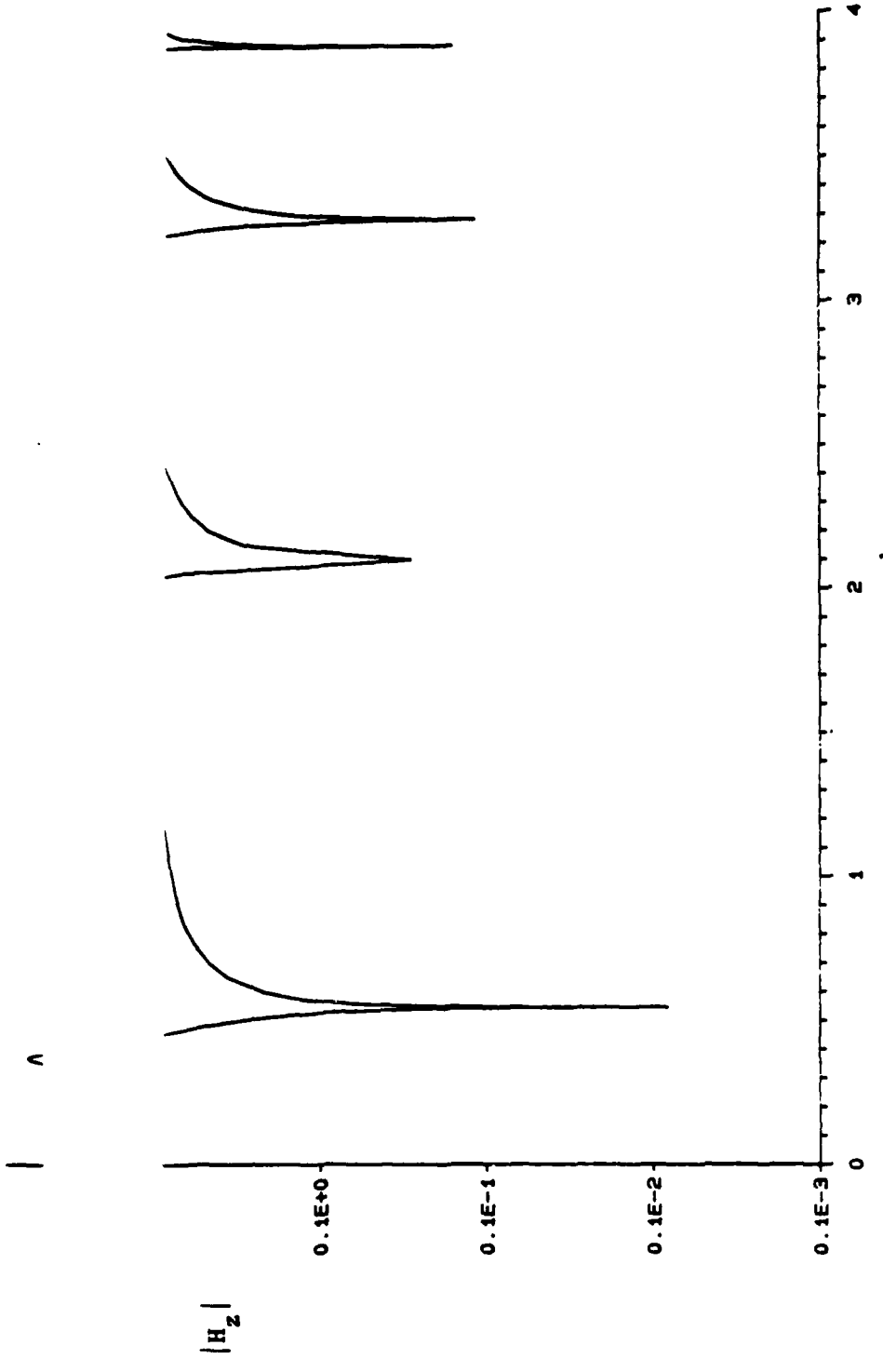


Fig. 9. Field amplitude $|H_z|$ at the center of the aperture for $\phi_o = 5°$ and $\alpha = 0°$ plotted on a logarithmic scale.

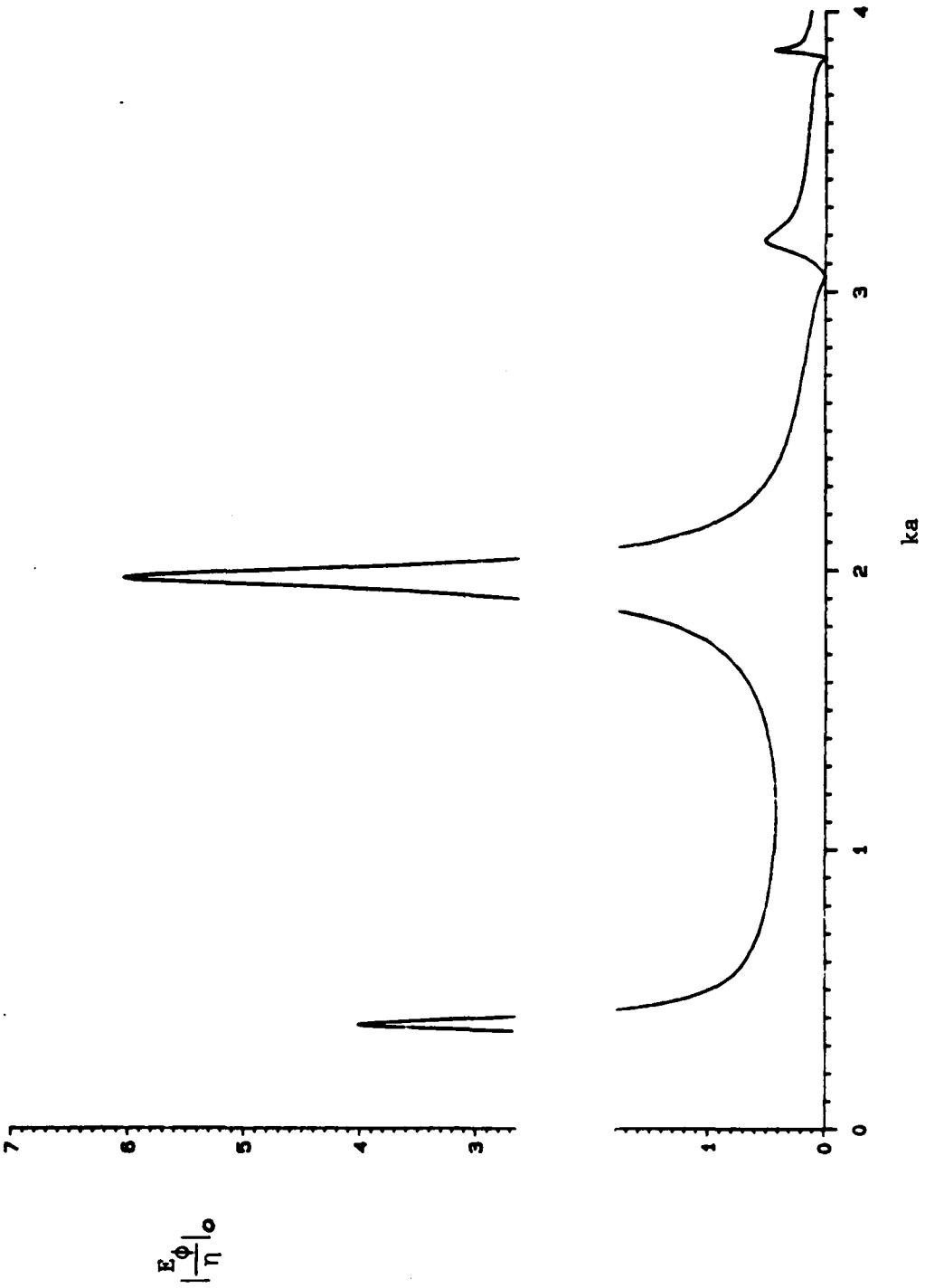


Fig. 10. Field amplitude $\left|\frac{E_\phi}{\eta}\right|_o$ at the center of the cylinder for $\phi_o = 5°$ and $\alpha = 0°$.

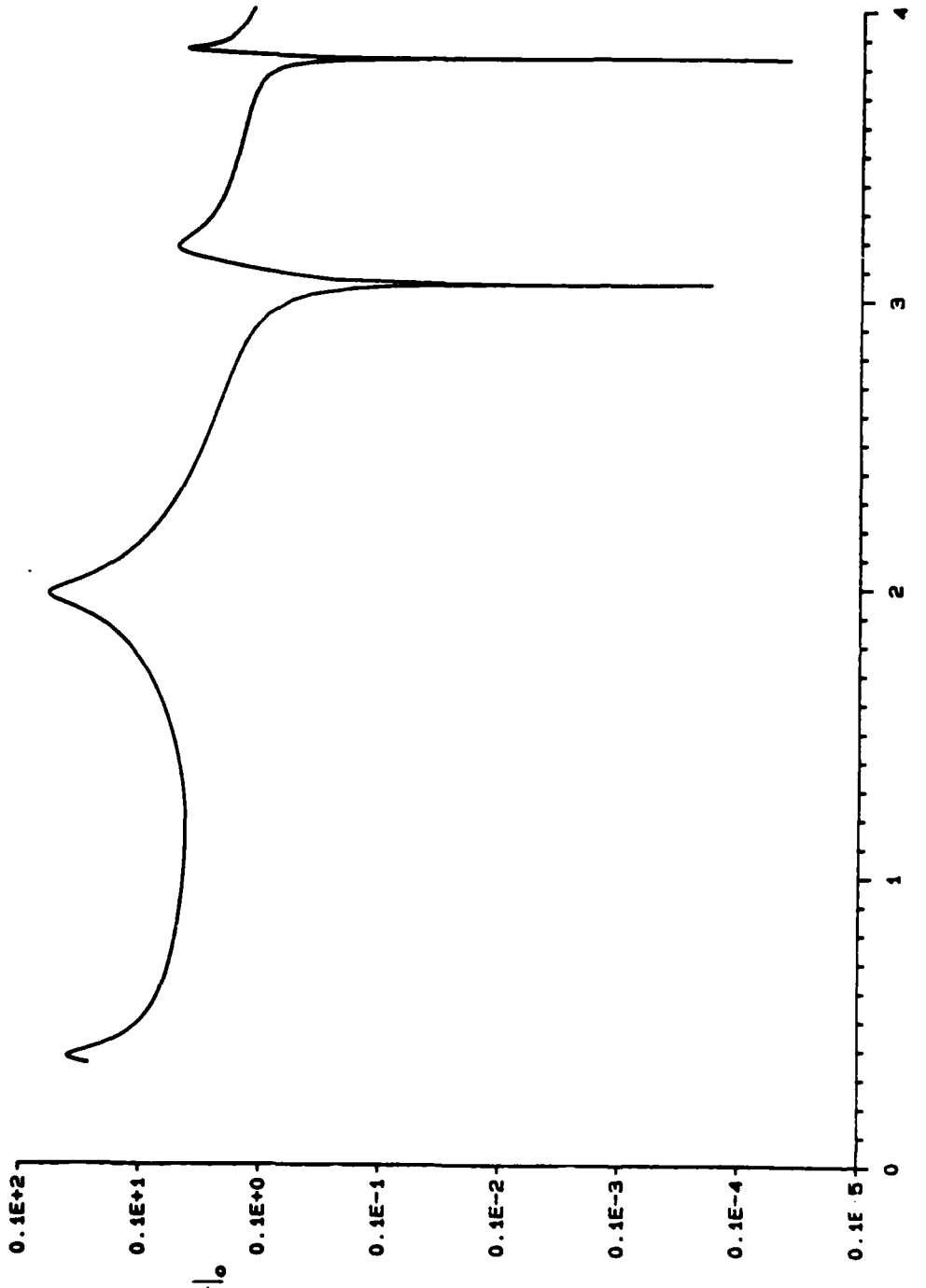


Fig. 11. Field amplitude $\left|\frac{E_\phi}{\eta}\right|_o$ at the center of the cylinder for $\phi_o = 5°$ and $\alpha = 0°$ plotted on a logarithmic scale.

Table 2. Field amplitudes $|E_\phi/\eta|_o$ and $|H_z|$ at the center of the cylinder for resonant values of ka. $\phi_o = 5°$ and $\alpha = 0°$. For comparison, $|E^A_\phi/\eta|_o$ of (86) and $|H^A_z|$ of (85) are also tabulated. The subscript "o" on $|E_\phi/\eta|$ and $|E^A_\phi/\eta|$ denotes evaluation at $\phi = 0°$.

| ka | $\lvert E_\phi/\eta\rvert_o$ | $\lvert E^A_\phi/\eta\rvert_o$ | $\lvert H_z\rvert$ | $\lvert H^A_z\rvert$ |
|---|---|---|---|---|
| 1.841184 | 1.606 | 1.604 | $3 \times 10^{-6}$ | 0.0 |
| 3.054237 | $2 \times 10^{-5}$ | 0.0 | $3 \times 10^{-5}$ | 0.0 |
| 3.831706 | $4 \times 10^{-6}$ | 0.0 | 4.826 | 4.829 |
| 4.20119 | $1 \times 10^{-4}$ | 0.0 | $3 \times 10^{-4}$ | 0.0 |
| 5.31755 | 0.018 | 0.0 | $3 \times 10^{-4}$ | 0.0 |
| 5.33144 | 2.824 | 2.822 | $5 \times 10^{-6}$ | 0.0 |

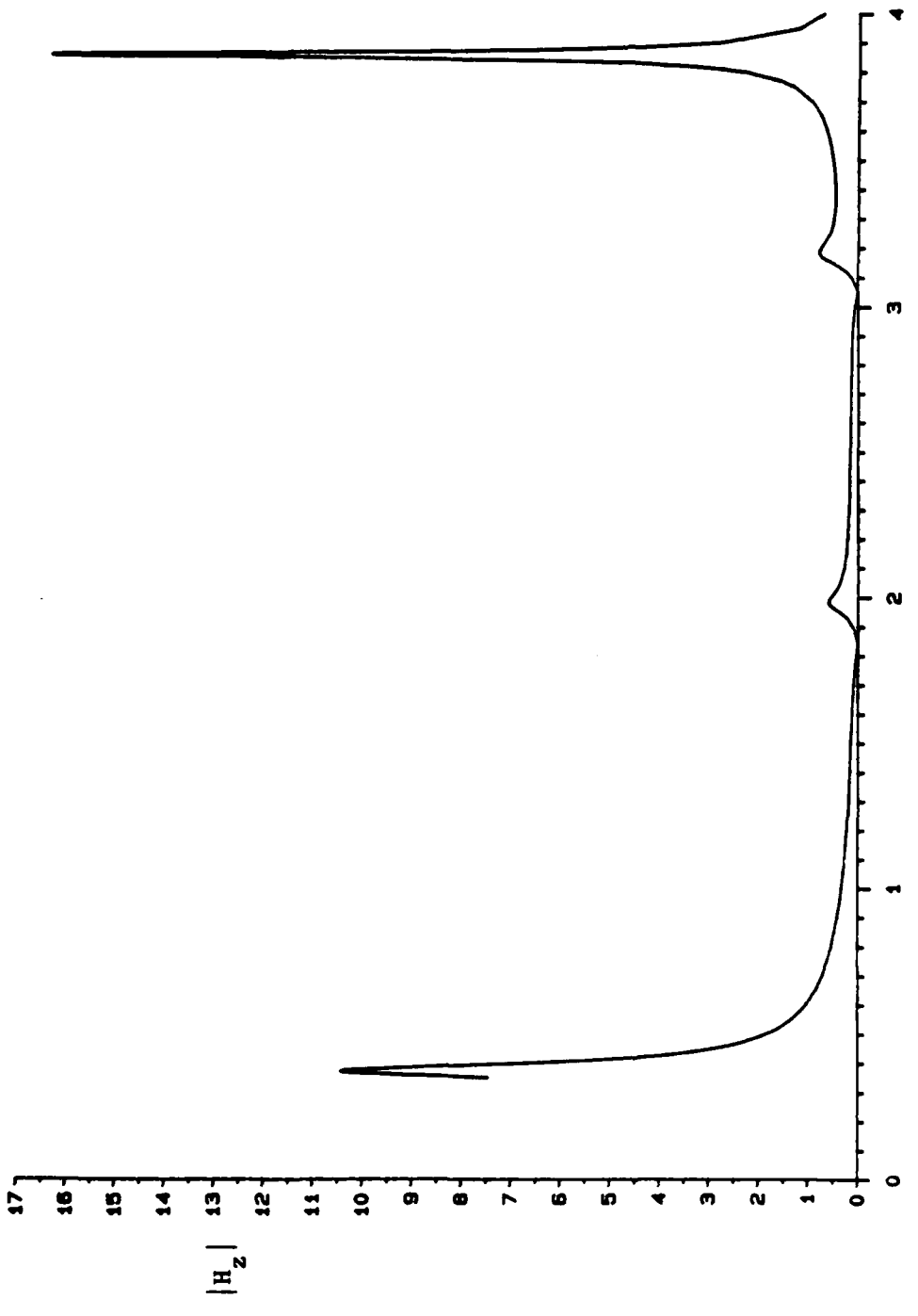


Fig. 12. Field amplitude $|H_z|$ at the center of the cylinder for $\phi_o = 5°$ and $\alpha = 0°$.

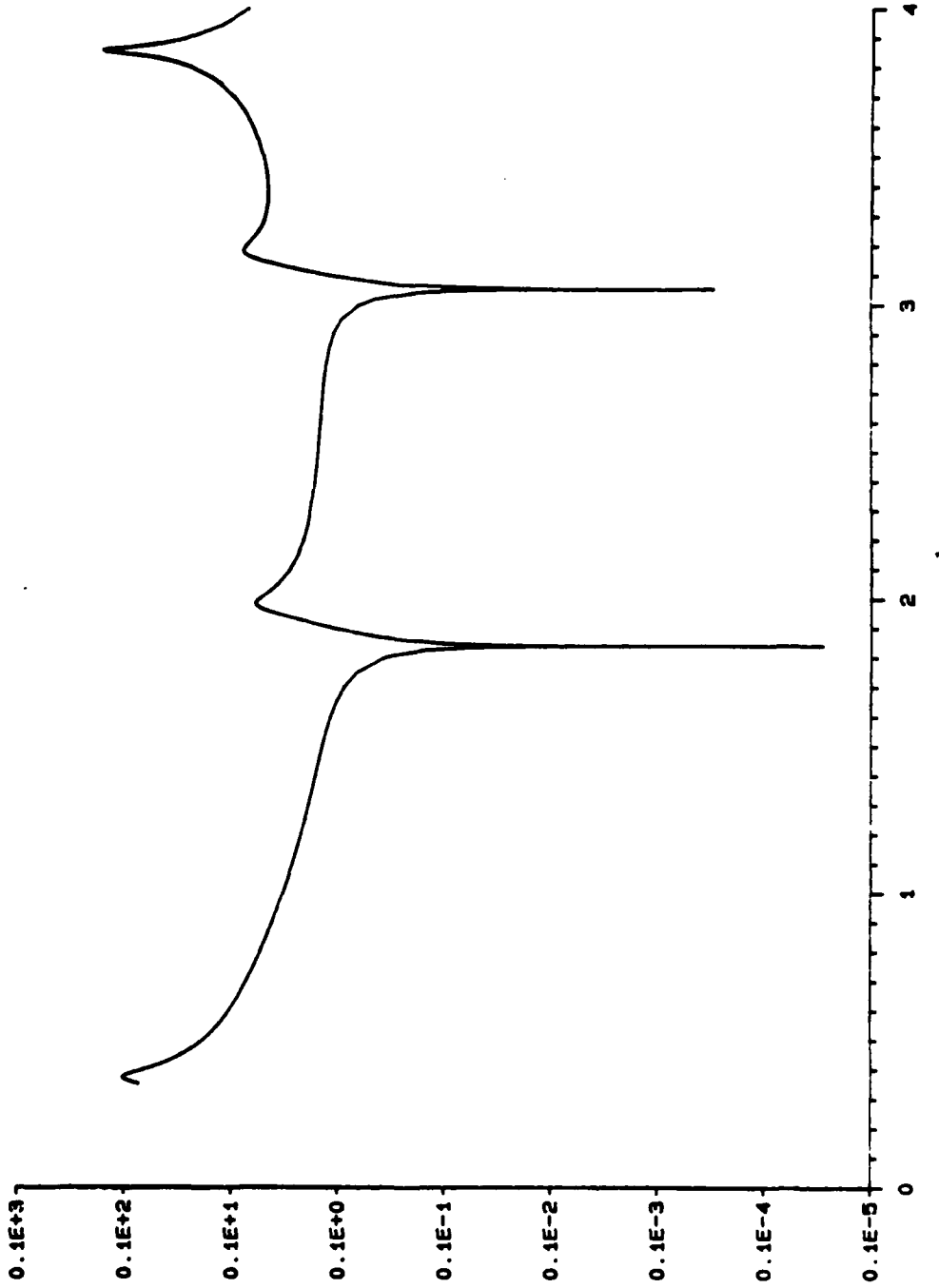


Fig. 13. Field amplitude $|H_z|$ at the center of the cylinder for $\phi_o = 5°$ and $\alpha = 0°$ plotted on a logarithmic scale.

The solid curve in Fig. 14 is a ka scan of the normalized back-scattering width $\sigma/\pi a$ of the cylinder of Fig. 6. This $\sigma/\pi a$ is given by (76) with $\phi = \alpha = 0°$. The dashed curve in Fig. 14 is the normalized back-scattering width of the corresponding closed cylinder, given by (77) with $\phi = \alpha = 0°$. Comparing the solid curve in Fig. 14 with that in the left-hand plot of [8, Fig. 19b], we note that the first peak of the solid curve in Fig. 14 is slightly higher than that of the solid curve in [8]. Furthermore, the spike in the neighborhood of ka = 5.32 is more pronounced on the solid curve of Fig. 14 than on the solid curve in [8].

In Fig. 15, the normalized forward scattering width $\sigma/\pi a$ of the cylinder of Fig. 6 is plotted solid and the normalized forward scattering width of the corresponding closed cylinder is plotted dashed. These scattering widths were calculated by setting $\phi = 180°$ and $\alpha = 0°$ in (76) and (77). Comparing the solid curve in Fig. 15 with that in the right-hand plot of [8, Fig. 19b], we observe that the spike in the neighborhood of ka = 5.32 protrudes down farther in Fig. 15 than in [8].

The solid curve in Fig. 16 is a ka scan of the normalized back-scattering width $\sigma/\pi a$ of the cylinder of Fig. 14 with $\alpha = 180°$ instead of $\alpha = 0°$. This $\sigma/\pi a$ is given by (76) with $\phi = \alpha = 180°$. The dashed curve in Fig. 16 is the normalized back-scattering width of the corresponding closed cylinder, given by (77) with $\phi = \alpha = 180°$. In Fig. 16, the aperture is in the shadow region whereas in Figs. 14 and 15, the aperture was directly illuminated. By reciprocity [15, p. 45], the forward scattering width of the cylinder of Fig. 16 is exactly the same as the forward scattering width of the cylinder of Fig. 14. Comparing the solid curve in Fig. 16 with that in [8, Fig. 21a], we observe that the first peak of the solid curve in Fig. 16 is slightly higher than that of the solid curve in [8].

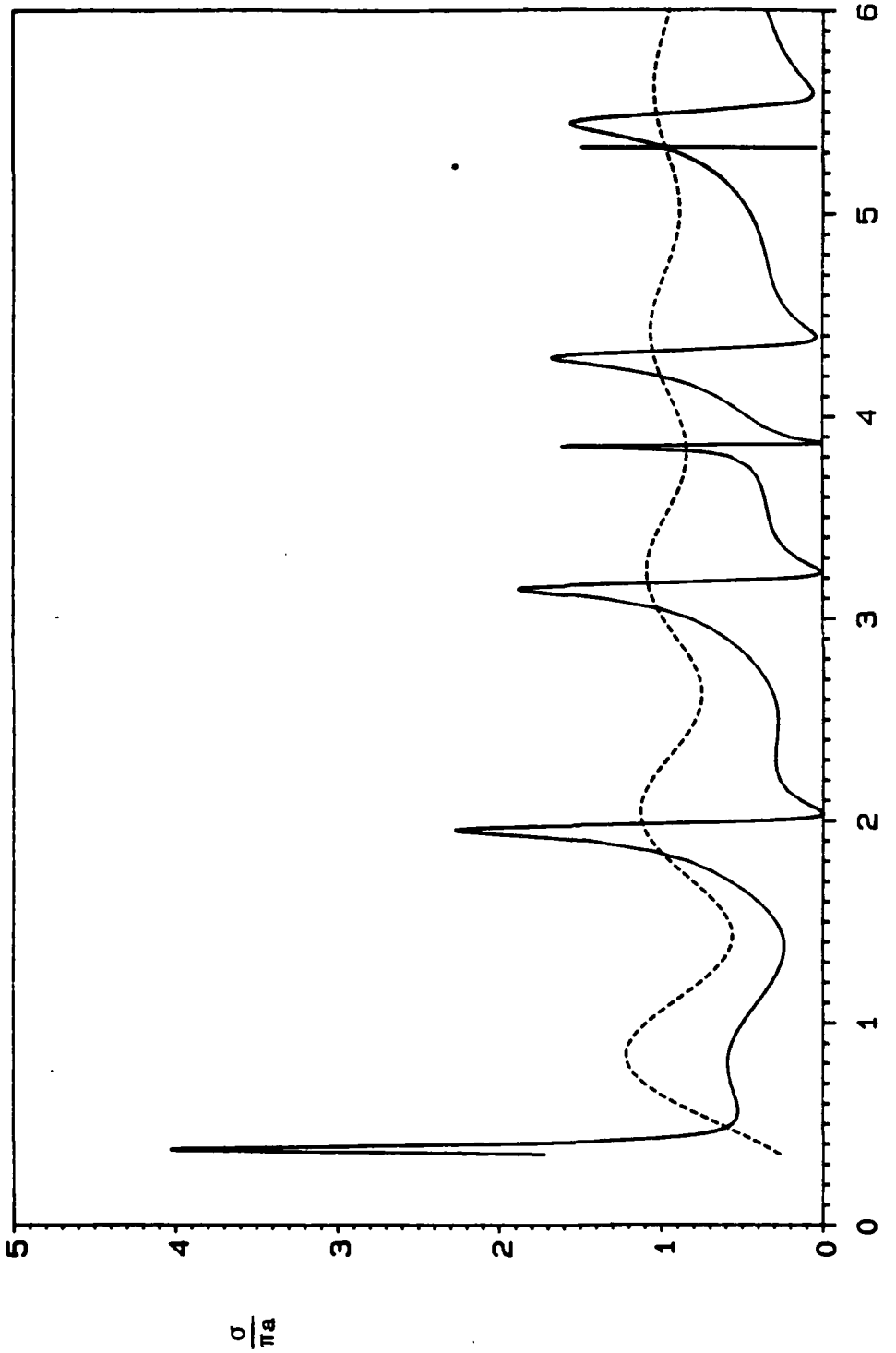


Fig. 14. Normalized scattering width σ/πa where σ is the back-scattering width of the cylinder of Fig. 6. σ/πa of the slit cylinder is shown solid. σ/πa of the corresponding closed cylinder is shown dashed.

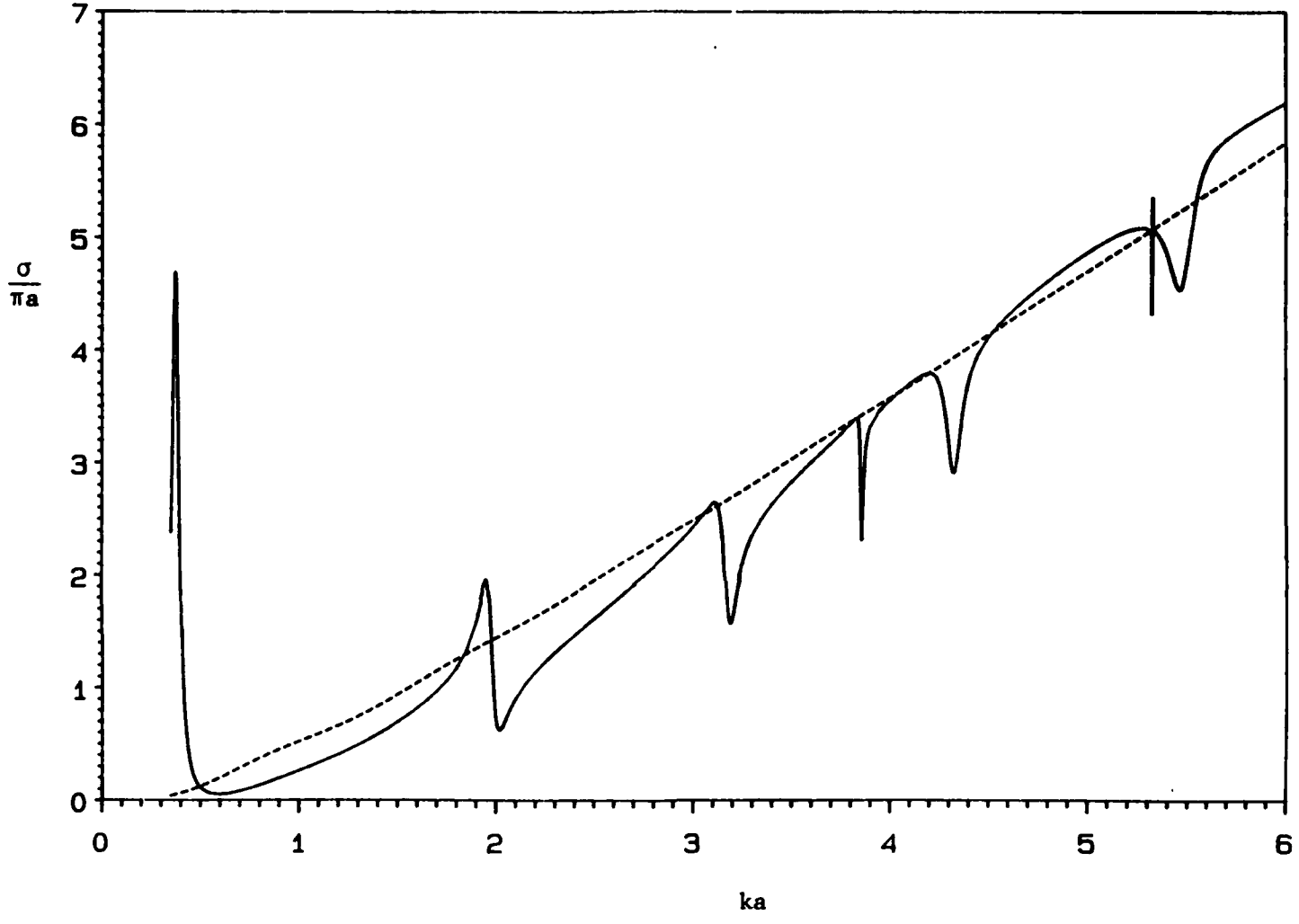


Fig. 15. Normalized scattering width $\sigma/\pi a$ where $\sigma$ is the forward scattering width of the cylinder of Fig. 6. $\sigma/\pi a$ of the slit cylinder is shown solid. $\pi/\sigma a$ of the corresponding closed cylinder is shown dashed.

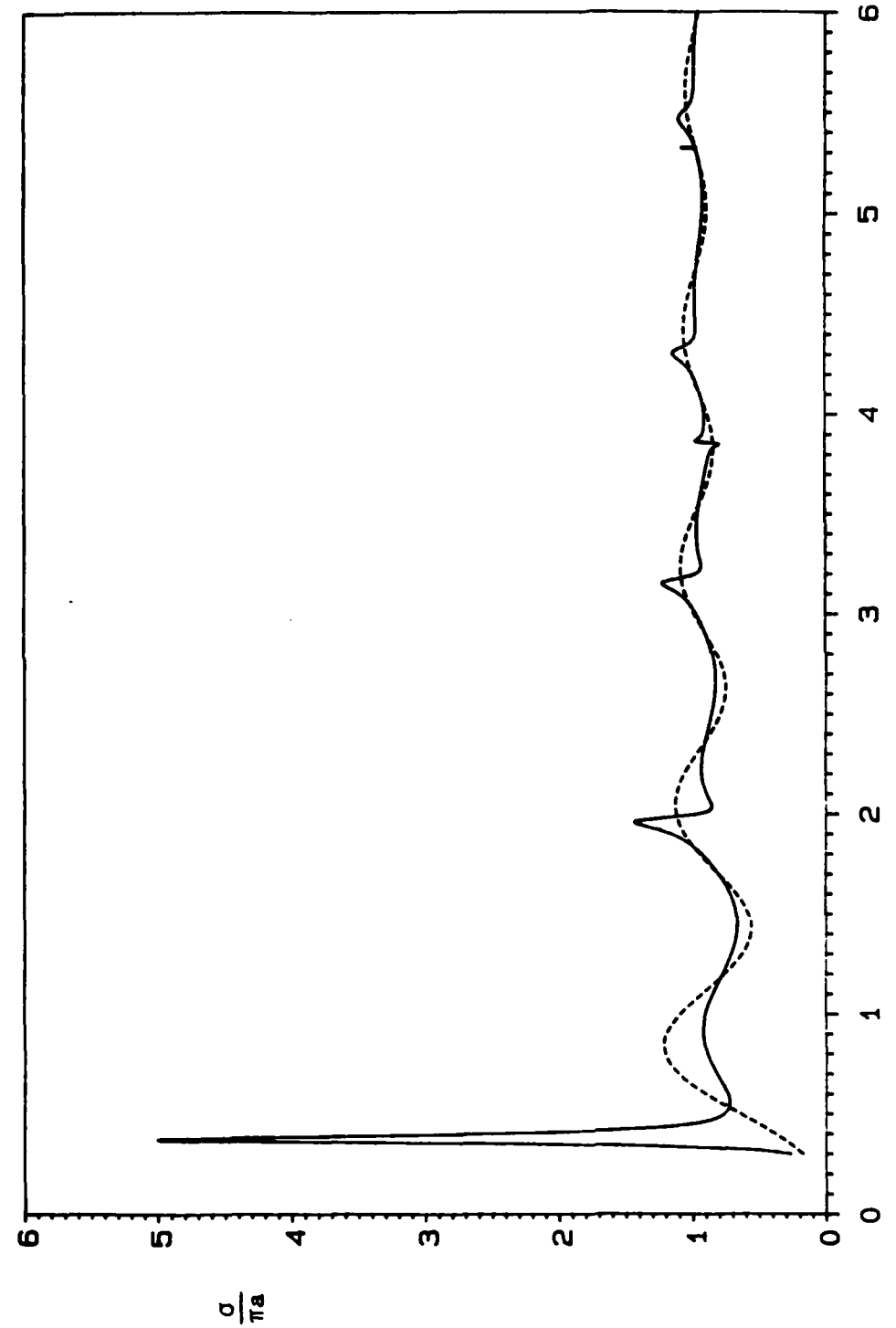


Fig. 16. Normalized scattering width $\sigma/\pi a$ where $\sigma$ is the back-scattering width of the cylinder of Fig. 6 with $\alpha = 180°$ instead of $\alpha = 0°$. $\sigma/\pi a$ of the slit cylinder is shown solid. $\sigma/\pi a$ of the corresponding closed cylinder is shown dashed.

In Section VI, it was shown that, at resonant values of ka, scattering from a cylinder with a narrow slit aperture is approximately the same as scattering from the corresponding closed cylinder. This means that the solid and dashed curves in each of Figs. 14, 15, and 16 should cross each other at values of ka very close to the resonant values of ka. Labelling the solid curve $\sigma/\pi a$ and the dashed curve $\sigma^{sc}/\pi a$, we computed $\sigma/\pi a$ and $\sigma^{sc}/\pi a$ of Figs. 14, 15, and 16 at the first six resonant values of ka, given in the first column of Table 1. Reassuringly, the difference between each of these values of $\sigma/\pi a$ and the corresponding value of $\sigma^{sc}/\pi a$ was always less than 1%. In Fig. 14, $\sigma/\pi a$ is correct at ka = 5.31755 and at ka = 5.33144 because it agrees with $\sigma^{sc}/\pi a$ there. Correctness of $\sigma/\pi a$ at these values of ka in Fig. 14 is meaningful because $\sigma/\pi a$ is changing so rapidly there. Reading our numerical values of $\sigma/\pi a$ in the neighborhood of ka = 5.32, we see that $\sigma/\pi a$ is 0.973 at ka = 5.31755, rises to 1.49 at ka = 5.32667, dips to 0.048 at ka = 5.326885, and then rises to 0.979 at ka = 5.33144!

The precise locations of the peaks of the solid curves in Figs. 14, 15, and 16 are pinpointed in Table 3. The entries in any column of Table 3 are the values of ka at the peaks of the solid curve in the figure whose number appears at the head of the column. Some spaces in Table 3 were left empty in order to obtain alignment of the abscissas of similar maxima.

Table 3. Values of ka at the peaks of the solid curves in Figs. 14, 15, and 16.

| Fig. 14 | Fig. 15 | Fig. 16 |
|---|---|---|
| 0.375 | 0.3725 | 0.3755 |
| 0.800 | | 0.91 |
| 1.958 | 1.952 | 1.96 |
| 2.30 | | 2.22 |
| 3.149 | 3.11 | 3.153 |
| | | 3.40 |
| 3.8535 | 3.83 | 3.866 |
| 4.292 | 4.20 | 4.305 |
| | 5.27 | 4.56 |
| 5.32667 | 5.32698 | 5.32677 |
| 5.444 | | 5.47 |
| | | 5.72 |

# APPENDIX A

## EVALUATION OF $S^e_{jn}$ AND $S^o_{jn}$

Changing the variable of integration from $\phi$ to

$$x = \phi/\phi_o \tag{A-1}$$

in (16) and (26), we obtain

$$S^e_{jn} = \frac{\varepsilon_n \phi_o}{2\pi} \int_{-1}^{1} \frac{x^{2j-2}\cos(bx)}{\sqrt{1-x^2}}\, dx \tag{A-2}$$

$$S^o_{jn} = \frac{\phi_o}{\pi} \int_{-1}^{1} \frac{x^{2j-1}\sin(bx)}{\sqrt{1-x^2}}\, dx \tag{A-3}$$

where

$$b = n\phi_o \tag{A-4}$$

In regard to (A-2) and (A-3), it is known that [17, formulas 3.752(2.) and 3.753(2.)]

$$\int_{-1}^{1} \sqrt{1-x^2}\cos(bx)\, dx = \frac{\pi J_1(b)}{b} \tag{A-5}$$

$$\int_{-1}^{1} \frac{\cos(bx)}{\sqrt{1-x^2}}\, dx = J_o(b) \tag{A-6}$$

Assuming that $n \neq 0$, comparison of (A-6) with (A-2) gives

$$S^e_{1n} = \phi_o J_o(b) \tag{A-7}$$

Integrating the right-hand side of (A-3) by parts, we obtain

$$S^o_{1n} = \frac{\phi_o b}{\pi} \int_{-1}^{1} \sqrt{1-x^2}\cos(bx)\, dx \tag{A-8}$$

which, in view of (A-5), reduces to

$$S^{o}_{1n} = \phi_o J_1(b) \tag{A-9}$$

Seeking a recurrence relation for $S^{e}_{jn}$ when $n \neq 0$, we use the identity

$$x^{2j-2} = x^{2j-4}(1 - (1-x^2)) \tag{A-10}$$

to recast (A-2) as

$$S^{e}_{jn} = S^{e}_{j-1,n} - \frac{\phi_o}{\pi} \int_{-1}^{1} x^{2j-4} \sqrt{1 - x^2} \cos (bx)\, dx \tag{A-11}$$

which, upon integration by parts, becomes

$$S^{e}_{jn} = S^{e}_{j-1,n} + \frac{\phi_o}{b\pi} \int_{-1}^{1} \sin (bx) \frac{d}{dx} (x^{2j-4} \sqrt{1 - x^2})\, dx \tag{A-12}$$

Performing the indicated differentiation in (A-12), we obtain

$$S^{e}_{jn} = S^{e}_{j-1,n} - \frac{(2j-3)}{b} S^{o}_{j-1,n} + \frac{2(j-2)}{b} S^{o}_{j-2,n}, \quad j=2,3,\ldots \tag{A-13}$$

where the $S^{o}_{j-2,n}$ term is to be omitted when j=2.

Seeking a recurrence relation for $S^{o}_{jn}$, we use an identity similar to (A-10) to recast (A-3) as

$$S^{o}_{jn} = S^{o}_{j-1,n} - \frac{\phi_o}{\pi} \int_{-1}^{1} x^{2j-3} \sqrt{1 - x^2} \sin (bx)\, dx \tag{A-14}$$

An integration by parts changes (A-14) to

$$S^{o}_{jn} = S^{o}_{j-1,n} - \frac{\phi_o}{\pi b} \int_{-1}^{1} \cos (bx) \frac{d}{dx} (x^{2j-3} \sqrt{1 - x^2})\, dx \tag{A-15}$$

Performing the indicated differentiation in (A-15), we obtain the recurrence relation

$$S^{o}_{jn} = S^{o}_{j-1,n} + \frac{2(j-1)}{b} S^{e}_{jn} - \frac{(2j-3)}{b} S^{e}_{j-1,n}, \quad j=2,3,\ldots \tag{A-16}$$

Using (A-13) and (A-16) to recur up from (A-7) and (A-9), we obtain

$$S_{1n}^{e} = \frac{bJ_o(b)}{n} \tag{A-17}$$

$$S_{2n}^{e} = \frac{bJ_o(b) - J_1(b)}{n} \tag{A-18}$$

$$S_{3n}^{e} = \frac{(b^2-3)(bJ_o - 2J_1)}{nb^2} \tag{A-19}$$

$$S_{4n}^{e} = \frac{(b^4-9b^2+60)\ bJ_o(b) - 3(b^4 - 11\ b^2 + 40)\ J_1(b)}{nb^4} \tag{A-20}$$

$$S_{1n}^{o} = \frac{bJ_1(b)}{n} \tag{A-21}$$

$$S_{2n}^{o} = \frac{(b^2-2)\ J_1(b) + bJ_o(b)}{nb} \tag{A-22}$$

$$S_{3n}^{o} = \frac{(b^4-7b^2+24)\ J_1(b) + 2b(b^2 - 6)\ J_o(b)}{nb^3} \tag{A-23}$$

$$S_{4n}^{o} = \frac{(b^6-15b^4 + 192b^2-720)\ J_1(b)+3b(b^4 - 17b^2+120)\ J_o(b)}{nb^5} \tag{A-24}$$

Expressions (A-19), (A-20), (A-22), (A-23), and (A-24) become indeninate as b approaches zero. When $b \leq 2$, we approximate cos (bx) in 2) by [18, formula 415.02].

$$\cos(bx) = 1 - \frac{b^2x^2}{2} + \frac{b^4x^4}{24} - \frac{b^6x^6}{720} + \frac{b^8x^8}{40320} - \frac{b^{10}x^{10}}{3628800} \tag{A-25}$$

encounter integrals $I_{2j}$ defined by

$$I_{2j} = \int_{-1}^{1} \frac{x^{2j}dx}{\sqrt{1-x^2}}, \quad j = 0,1,2,\ldots \tag{A-26}$$

is evident from [17, formula 3.248(3.)] that

$$I_{2j} = \frac{\pi(2j-1)!!}{(2j)!!}, \quad j=0,1,2,\ldots \tag{A-27}$$

re

$$(2j-1)!! = \begin{cases} 1 & , j = 0 \\ 1\cdot3\cdot5 \ldots 2j-1, & j \geq 1 \end{cases} \tag{A-28}$$

and

$$(2j)!! = \begin{cases} 1 & , \quad j = 0 \\ 2\cdot 4\cdot 6\ldots 2j & , \quad j \geq 1 \end{cases} \tag{A-29}$$

From (A-27), we obtain

$$\begin{aligned} I_o &= \pi \\ I_2 &= \pi/2 \\ I_4 &= 3\pi/8 \\ I_6 &= 5\pi/16 \\ I_8 &= 35\pi/128 \\ I_{10} &= 63\pi/256 \\ I_{12} &= 231\pi/1024 \\ I_{14} &= 429\pi/2048 \\ I_{16} &= 6435\pi/32768 \\ I_{18} &= 12155\pi/65536 \end{aligned} \tag{A-30}$$

In view of (A-30), substitution of (A-25) into (A-2) gives

$$S_{1n}^e = \frac{\varepsilon_n \phi_o}{2}\left[1 - \frac{b^2}{4} + \frac{b^4}{64} - \frac{b^6}{2304} + \frac{b^8}{147456} - \frac{b^{10}}{14745600}\right] \tag{A-31}$$

$$S_{2n}^e = \frac{\varepsilon_n \phi_o}{4}\left[1 - \frac{3b^2}{8} + \frac{5b^4}{192} - \frac{7b^6}{9216} + \frac{b^8}{81920} - \frac{11b^{10}}{88473600}\right] \tag{A-32}$$

$$S_{3n}^e = \frac{3\varepsilon_n \phi_o}{16}\left[1 - \frac{5b^2}{12} + \frac{35b^4}{1152} - \frac{7b^6}{7680} + \frac{11b^8}{737280} - \frac{143b^{10}}{928972800}\right] \tag{A-33}$$

$$S_{4n}^e = \frac{5\varepsilon_n \phi_o}{32}\left[1 - \frac{7b^2}{16} + \frac{21b^4}{640} - \frac{77b^6}{76800} + \frac{143b^8}{8601600} - \frac{143b^{10}}{825753600}\right] \tag{A-34}$$

When $b \leq 2$, we approximate sin (bx) in (A-3) by [18, formula 415.01]

$$\sin(bx) = bx - \frac{b^3x^3}{6} + \frac{b^5x^5}{120} - \frac{b^7x^7}{5040} + \frac{b^9x^9}{362880} - \frac{b^{11}x^{11}}{39916800} \tag{A-35}$$

We substitute (A-35) into (A-3) and use (A-30) in order to obtain

$$S_{1n}^{o} = \frac{\phi_o b}{2}\left[1 - \frac{b^2}{8} + \frac{b^4}{192} - \frac{b^6}{9216} + \frac{b^8}{737280} - \frac{b^{10}}{88473600}\right] \tag{A-36}$$

$$S_{2n}^{o} = \frac{3\phi_o b}{8}\left[1 - \frac{5b^2}{36} + \frac{7b^4}{1152} - \frac{b^6}{7680} + \frac{11b^8}{6635520} - \frac{13b^{10}}{928972800}\right] \tag{A-37}$$

$$S_{3n}^{o} = \frac{5\phi_o b}{16}\left[1 - \frac{7b^2}{48} + \frac{21b^4}{3200} - \frac{11b^6}{76800} + \frac{143b^8}{77414400} - \frac{13b^{10}}{825753600}\right] \tag{A-38}$$

$$S_{4n}^{o} = \frac{35\phi_o b}{128}\left[1 - \frac{3b^2}{20} + \frac{11b^4}{1600} - \frac{143b^6}{940800} + \frac{143b^8}{72253440} - \frac{17b^{10}}{1000432246}\right] \tag{A-39}$$

# REFERENCES

[1] J. A. Beren, "Diffraction of an H-polarized electromagnetic wave by a circular cylinder with an infinite axial slot," Ph.D. dissertation, University of Arizona, Tucson, 1977.

[2] J. A. Beren, "Diffraction of an H- polarized electromagnetic wave by a circular cylinder with an infinite axial slot," IEEE Trans. Antennas Propagat., vol. AP-31, pp. 419-425, May 1983.

[3] E. V. Zakharov and Yu. V. Pimenov, "Numerical analysis of diffraction of electromagnetic waves by an open circular-cylindrical surface," Radiophysics and Quantum Electronics, vol. 22, pp. 426-431, May 1979.

[4] V. N. Koshparënok and V. P. Shestopalov, "Diffraction of a plane electromagnetic wave by a circular cylinder with a longitudinal slot," USSR Comput. Math. & Math. Phys., vol. 11, pp. 222-243, 1971.

[5] W. A. Johnson, "The scattering of an H-polarized plane wave from an axially slotted infinite cylinder: A dual series approach," Radio Sci., vol. 19, pp. 275-291, Jan.-Feb. 1984.

[6] R. W. Ziolkowski, W. A. Johnson, and Kendall F. Casey, "Applications of Riemann-Hilbert problem techniques to electromagnetic coupling through apertures," Radio Sci., vol. 19, pp. 1425-1431, Nov.-Dec. 1984.

[7] R. W. Ziolkowski, "n-series problems and the coupling of electromagnetic waves to apertures: A Riemann-Hilbert approach," SIAM J. Math. Anal., vol. 16, pp. 358-378, March 1985.

[8] R. W. Ziolkowski and J. B. Grant, "Scattering from cavity-backed apertures: The generalized dual series solution of the concentrically loaded E-pol slit cylinder problem," IEEE Trans. Antennas Propagat., vol. AP-35, pp. 504-528, May 1987.

[9] P. M. Morse and H. Feshbach, Methods of Theoretical Physics. New York: McGraw-Hill, 1953.

[10] M. Abramowitz and I. A. Stegun, Handbook of Mathematical Functions (Natl. Bur. Std. U. S. Appl. Math. Ser. 55). Washington, D. C.: U. S. Govt. Printing Office, 1964.

[11] J. R. Mautz and R. F. Harrington, "Electromagnetic penetration into a conducting circular cylinder through a narrow slot, TM case," Report SYRU/DECE/TR-86/4, Department of Electrical and Computer Engineering, Syracuse University, Syracuse, NY 13244-1240, Dec. 1986.

[12] J. R. Mautz and R. F. Harrington, "Computer program for electromagnetic penetration into a conducting circular cylinder through a narrow slot, TM case," Report SYRU/DECE/TR-87/1, Department of Electrical and Computer Engineering, Syracuse University, Syracuse, NY 13244-1240, Feb. 1987.

[13] K. Y. Kabalan, R. F. Harrington, H. A. Auda, and J. R. Mautz, "Characteristic modes for slots in a conducting plane, TE case," IEEE Trans. Antennas Propagat., vol. AP-35, pp. 162-168, Feb. 1987.

[14] R. F. Harrington, Time-Harmonic Electromagnetic Fields. New York: McGraw-Hill, 1961.

[15] R. F. Harrington, Field Computation by Moment Methods. New York: Macmillan, 1968.

[16] Yuan, X., "Electromagnetic coupling into slotted TE and TM cylindrical conductors by the pseudo-image method," Ph.D. dissertation, Syracuse University, Syracuse, NY 13244-1240, Nov. 1987.

[17] I. S. Gradshteyn and I. M. Ryzhik, Table of Integrals, Series, and Products. New York: Academic Press, 1965.

[18] H. B. Dwight, Tables of Integrals and Other Mathematical Data. New York: Macmillan, 1961.

END

DATE

FILMED

5-88

DTIC